ChemComm

REVIEW ARTICLE

View Article Online
View Journal | View Issue

Cite this: *Chem. Commun.*, 2026, **62**, 4477

Diverse hydrogen chemistry with perspectives for energy storage

Colin J. Webb, [a] Terry D. Humphries, [b] Joseph A. Teprovich, [c] Marek Polanski, [d] Michael Heere, [e] Hai-Wen Li, [f] Michael Felderhoff, [g] Yaroslav Filinchuk, [h] Martin Dornheim, *[i] Mark Paskevicius, [b] Craig E. Buckley [b] and Torben R. Jensen *[j]

The chemistry of hydrogen and its interaction with matter is remarkably diverse with new discoveries and materials continuously being uncovered. New types of chemical bonding and interactions allow for the preparation of new compounds with unusual compositions and properties. For instance, neutral hydrogen molecules may spontaneously form penta-dihydrogen clusters, $(H_2)_5$, in nanoporous materials with extremely dense packing, similar to metallic hydrogen at high pressure. Hydrides with extreme hydrogen densities – 'superhydrides' – have yielded record critical temperatures under pressure and now guide routes toward low-pressure high-temperature hydride superconductors. A well-known weak interaction identified in biological matter, the hydrogen bond, has an inorganic analogue: the dihydrogen bond. These two interactions have very similar bond lengths and bond strengths that are known to produce flexible and relatively open structures, which often have interesting functionalities. Recently, the di-hydrogen bond has come into focus for development of fast divalent magnesium and calcium cationic conductors. In this review, we highlight key advances in the synthesis and characterisation of novel hydrogen-based materials and illustrate how the compositional and structural versatility of hydrides leads to new functionalities. Hydrides are highly relevant materials with a diversity of energy applications such as solid-state hydrogen storage, solid-state batteries and superconductors, as well as future global hydrogen transportation.

Received 13th October 2025,
Accepted 19th January 2026

DOI: 10.1039/d5cc05834a

rsc.li/chemcomm

1. Introduction

Hydrogen is the lightest and simplest element and exists as the smallest molecule with only two electrons. However, hydrogen can interact with other elements and compounds by forming a wide variety of bonding types spanning stronger covalent, ionic and metallic bonding along with different types of weaker interactions. In this highlight, we discuss how these weak interactions can lead to new materials and properties, which may help address global challenges such as solid-state energy storage. In addition, stronger interactions may provide hydrogen-based energy storage in the solid-state for mobile applications and large-scale energy transportation.[1–7]

Complex hydrides can be synthesised from some late transition metals, *i.e.* Fe, Ni and Co,[8,9] and some p-block elements, such as boron, aluminium and nitrogen.[4,7,10] In particular, boron-based materials have received significant interest over the past decade owing to their fascinating structural chemistry and diversity of compositions and properties.[10] Many of these compounds have very high hydrogen densities with potential for solid-state hydrogen storage. Ammonium borohydride, NH_4BH_4, which is isoelectronic to natural gas, has attained significant attention owing to its extreme gravimetric hydrogen density.[11,12] The physical and chemical properties of this material can be modified by additional reactions with more stable metal borohydrides, $M(BH_4)_x$, to form $(NH_4)_yM(BH_4)_x$.[13] Other types of compounds with extremely high hydrogen content can also be produced under high pressure (>1 GPa), called

[a] *School of Environment and Science, Griffith University, Brisbane, Australia*
[b] *Physics and Astronomy, School of Electrical Engineering, Computing and Mathematical Sciences, Curtin University, GPO Box U1987, Perth, WA 6845, Australia*
[c] *Department of Chemistry & Biochemistry, California State University Northridge, Northridge, CA 91330, USA*
[d] *Faculty of New Technologies and Chemistry, Military University of Technology, Kaliskiego 2 Str., 00-908 Warsaw, Poland*
[e] *TU Braunschweig, Institute of Internal Combustion Engines and Fuel Cells, Germany*
[f] *School of Advanced Energy, Sun Yat-sen University, Shenzhen 518107, China*
[g] *Department of Heterogeneous Catalysis, Max-Planck-Institut für Kohlenforschung, Kaiser-Wilhelm-Platz 1, 45470 Mülheim an der Ruhr, Germany*
[h] *Institute of Condensed Matter and Nanosciences, Université catholique de Louvain, 1348 Louvain-la-Neuve, Belgium*
[i] *Advanced Materials Research Group, Faculty of Engineering, University of Nottingham, Nottingham, NG7 2TU, UK. E-mail: Martin.Dornheim@nottingham.ac.uk*
[j] *Department of Chemistry and Interdisciplinary Nanoscience Center, Aarhus University, Langelandsgade 140, 8000 Aarhus C, Denmark. E-mail: trj@chem.au.dk*

'superhydrides'. Some of these compounds have unique properties such as high-temperature superconductivity.[14]

Recently, weak interactions and low dimensional frameworks have been shown to have structural flexibility and very high divalent cationic conductivity. The progress in the field has been partially driven by the successful development of new synthesis strategies, *e.g.* combining several approaches such as solvent-based methods, solid–gas reactions and also mechanochemistry methods, enabling reactions under more extreme conditions, *i.e.* high temperature and pressure.[15]

Dihydrogen interactions, $H^{\delta-}\cdots H^{\delta+}$, can occur between partly positively charged hydrogen, $H^{\delta+}$ bonded to N, and partly negatively charged hydrogen, $H^{\delta-}$ bonded to B, as found in ammine metal hydroborate structures (Fig. 1).[16] A theoretical investigation of dihydrogen bonds revealed that $N–H^{\delta+}\cdots{}^{-\delta}H–B$ in $Mg(BH_4)_2{\cdot}NH_3$ has a bond energy of $\sim$20 kJ mol^{-1} and bond lengths of $\sim$2 Å.[17] This is very similar to hydrogen bonds known from biological matter, *i.e.* proteins, DNA, and membranes. Initially, dihydrogen interactions were considered as a means to tune hydrogen release from solids. However, there is no direct relation between dihydrogen bond strength (energy), $N–H^{\delta+}\cdots{}^{-\delta}H–B$, in the solid-state and the composition of the released gas from ammine metal borohydrides.[18]

Nanoporous materials are potential candidates for hydrogen gas storage, due to their high surface area and tuneable pore structure. In contrast to absorption, where a chemical interaction occurs between the hydrogen atom and a material, adsorption involves the binding of hydrogen molecules to the internal surfaces of porous solids through van der Waals interactions,[19] which is typically fast and readily reversed when the applied hydrogen pressure is removed.[20]

2. Porous materials for hydrogen adsorption

Molecules can adsorb to an interface by weak dispersion/van der Waals interactions,[19] which are proportional to the number of electrons and the molecular surface area. Thus, molecular hydrogen (H_2), the smallest molecule of all with only two electrons, forms the weakest dispersion interactions with solid matter. A wide variety of adsorptive materials, including carbons such as graphite and nanotubes, activated carbons (AC), covalent organic frameworks (COFs), and metal–organic frameworks (MOFs),[20,21] among others, have been investigated. Pore size and pore volume affect the hydrogen storage capacity since micropores ($<$2 nm) increase the binding potential, while mesopores and hierarchical structures facilitate hydrogen diffusion and access, balancing storage density and kinetics.[21]

2.1. Challenges for storing hydrogen in porous materials

While hydrogen storage in porous materials generally requires less costly heat management than intermetallics, and some materials such as carbon are abundant and relatively inexpensive, there are still several disadvantages. The inherently low enthalpy of adsorption, typically around -4 to -8 kJ mol^{-1} for physisorption in materials such as activated carbons and many MOFs, requires a low or cryogenic temperature, usually 77 K, to obtain usable hydrogen capacities. This increases system costs through additional energy requirements of cooling and the supply of liquid nitrogen which increases the complexity of the storage system. This leads to the need for tank insulation and further heat management, thereby reducing the economic feasibility of large-scale implementation.

The cost of materials, due to their synthesis and processing can also be high. While activated carbons can be typically produced relatively inexpensively from biomass or synthetic precursors, metal-organic frameworks (MOFs) and covalent organic frameworks (COFs) often rely on costly organic linkers and metals.[22,23] Typical MOFs such as MOF-5[24] or HKUST-1[25] have promising storage capacities in laboratory experiments, but the cost of raw materials and the complexity of the synthesis processes when scaling to commercial quantities are still too high.[26] Suggested methods for industrial-scale MOF production to improve sustainability and reduce energy costs have included assessment of MOF life cycles as well as the component costs, toxicity, safety, washing and activation.[23]

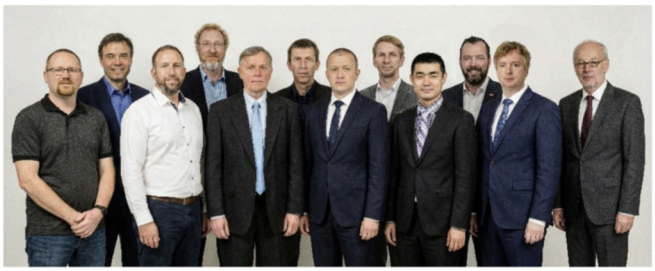

Group photo

The authors have for decades shared an interest in metal hydrides as 'energy materials'. They have synthesised a wide range of new intriguing hydrogen-based materials with interesting structures and compositions, including new types of bonding and hydrogen interactions with matter. These materials also have a variety of interesting properties that range from superconductivity, nanoscale porosity and outstanding divalent cationic conductivity, to solid-state hydrogen storage. There are also potential new applications of these materials in large scale, long-range solid-state energy storage, hydrogen compression and novel types of solid-state batteries based on abundant divalent metals, such as magnesium, calcium or zinc. These authors play a leading role in the hydrogen community by organising major conferences and summer schools and participating in the International Energy Agency hydrogen related tasks. Here, we illustrate that hydrogen is an important element for the future.

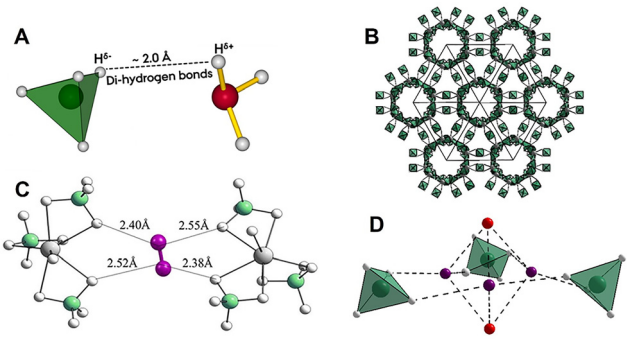

Fig. 1 (A) A di-hydrogen bond formed between partly negative hydrogen bonded to boron and partly positive hydrogen bonded to nitrogen. (B) The 'empty' nanoporous structure of γ-$Mg(BH_4)_2$. The structure contains 1D channels of ~9 Å diameter with apertures of ~5.8 Å. (C) The hydrogen molecules form directional hexa-hydrogen bonds, $(B–H^{\delta-})_2\cdots H–H\cdots(H^{\delta-}–B)_2$ with partially negatively charged hydrogen in the nanoporous framework (calculated with density functional theory methods). (D) Penta-dihydrogen clusters in the structure of γ-$Mg(BH_4)_2{\cdot}2.33H_2$ formed by five hydrogen molecules, $(H_2)_5$. Three hydrogen molecules (purple) in the penta-dihydrogen clusters are also forming hexa-hydrogen bonds, whereas the other two (red) only interact with the porous framework *via* weak dispersion interactions and behave as free rotors that rotate freely around their centre of mass. Colour code: boron is green and BH_4^- is shown as a tetrahedron, hydrogen is white and magnesium is shown as larger grey spheres. Fig. 1C and D are adapted from reference no. 47 with permission from Springer, Nature Chemistry, Volume 16, 2024, 809–816, copyright 2026 under a Creative Commons Attribution 4.0 International License.

The volumetric capacity of porous materials is typically low, although the gravimetric capacity can be significant due to high surface areas. Volumetric hydrogen capacity, which is more important for mobile applications such as fuel cell vehicles, is limited by the low density of many porous materials. The porous material can be compacted or densified by pressing into discs or pellets; however, this can reduce the porosity and restrict the diffusion of hydrogen gas.[27] Nanoporous materials adsorb hydrogen readily at low pressures; consequently, the majority of the hydrogen capacity is only released when the pressure is substantially reduced, typically lower than that required by fuel cells, meaning that the usable capacity is much lower than the full laboratory capacity reported in the literature.[21] This may be improved by applying temperature–pressure swings, increasing the temperature of the vessel to increase the hydrogen back pressure to a usable value for a fuel cell.[28]

In addition, repeated adsorption–desorption cycles can damage the structural stability of some materials such as MOFs. For example, under mechanical stress due to the pelletisation necessary in the forming process, the porous framework of some MOFs may collapse or pores can be blocked, reducing the cycling capacity and operational lifetime.[29] Research on more robust frameworks, particularly those with strong metal–ligand bonds, is on-going. Forming composite materials, where MOFs are combined with polymers or carbons, has been proposed to improve structural integrity while retaining a high surface area.[20,30]

At the system level, managing the application and removal of heat during adsorption and desorption, respectively, is another challenge for reducing costs. Efficient thermal management allows the maintenance of equilibrium pressures and prevents delays in fuelling and discharging.

2.2. Pore size, hydrogen density and increasing the hydrogen capacity

The relationship between pore size, hydrogen density, and overall storage capacity has been the subject of intensive investigation.[28] Hydrogen adsorption is strongly influenced by confinement effects: at low pressures in narrow micropores (<1 nm), the overlap of potential energy fields from pore walls increases the binding energy compared to flat surfaces, effectively increasing local hydrogen density. At higher pressures, the maximum uptake is approximately proportional to the total pore volume.

The total hydrogen capacity is determined by the area of the surface and the volume of pores available to hydrogen molecules, as well as the interaction of the hydrogen with the surface material under the applied pressure and temperature conditions. For adsorption largely defined by surface interactions, the excess hydrogen adsorption (the amount of hydrogen adsorbed on a material's surface beyond what would occupy the same pore volume as compressed bulk gas) scales with the surface area and has a maximum of approximately 1 wt% per 500 $m^2\ g^{-1}$ at 77 K, known as Chahine's Rule,[31] see Fig. 2. The maximum uptake at cryogenic temperatures typically occurs at hydrogen pressures of 20–50 bar. For microporous materials, the pore dimensions affect the density of hydrogen stored in the pore volume. Experimental studies employing the same porous activated carbon and carbide-derived carbon (but with different pore diameters) indicate that mesopores (pore sizes > ~25 nm)

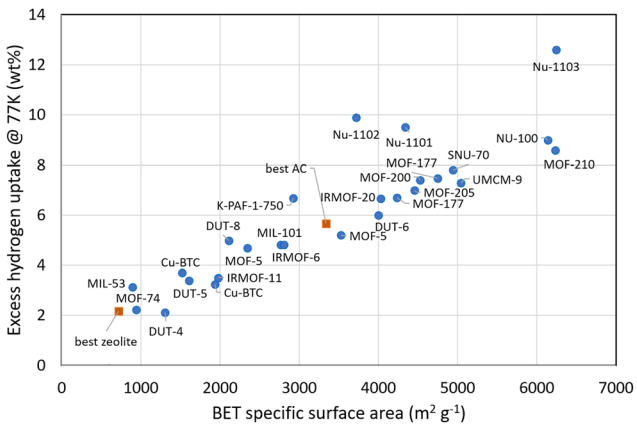

Fig. 2 Excess gravimetric hydrogen uptake for various MOFs at 20 bar or above and 77 K (data shown as circles). For comparison, the data for the best zeolite and activated carbon (AC) are also included (data shown as squares). The slope is approximately 1 wt% per 500 $m^2\ g^{-1}$, showing Chahine's Rule. Adapted from Broom *et al.*[20] with permission from Springer, Applied Physics A, Volume 122, 2016, 151, copyright 2026 under the terms of the Creative Commons Attribution 4.0 International License (https://creativecommons.org/licenses/by/4.0), with additional data from Li *et al.*[34] and Ahmed *et al.*[35]

contribute very little to the hydrogen storage capacity and the majority of hydrogen is stored in micropores below 1.5 nm.[32] Overall, pore sizes of 0.6–0.7 nm give the optimal uptake per unit surface area.[33]

For a typical (rigid) microporous material, increasing the pressure of hydrogen increases the hydrogen content until a saturation is reached, yielding the type I isotherm. Higher temperatures reduce the adsorption capacity, and therefore, higher pressures are required to reach saturation. The density of hydrogen in the pores at the maximum capacity depends on both temperature and the nature of the gas–solid interaction. Efforts to determine the average density of hydrogen in a microporous material involve high pressure adsorption measurements substantially beyond the maximum capacity. At hydrogen pressures greater than that needed for saturation, a linear relationship between excess uptake and gas density allows the determination of the volume of the adsorbate, and hence the average density. For MOF materials at 77 K and pressures up to 4 MPa, the average density of hydrogen in the micropores was determined to be 50–70 g H_2 L^{-1}, approaching the density of liquid hydrogen, 71 g L^{-1}.[36] More recently, much higher pressures, up to 2000 bar, have been employed to investigate the hydrogen density in activated carbon at ambient temperature, yielding an average adsorbate density of 44.7 g H_2 L^{-1} (compared to 38.7 g H_2 L^{-1} for pure hydrogen gas at that pressure). This lower value reflects the much higher temperature (*cf.* 77 K), but still indicates that a higher capacity than that due to pressure alone is possible in porous materials at ambient temperature if the pressure is sufficiently high.[37]

Strategies to increase storage capacity of hydrogen physisorption include maximising a material's surface area, increasing pore volume and tailoring pore size distributions, introducing functional groups to strengthen interactions, doping with metal ions, catenation and incorporating open metal sites within MOFs. Open metal sites provide localised electrostatic interactions, which can increase adsorption enthalpies to greater than −15 kJ mol^{-1}.[38] Materials such as Co-based SNU-15 MOF with open Co(II) sites have demonstrated this effect, although the hydrogen uptake is only 0.74 wt% owing to the low density of metal sites.[39] Additionally, doping carbon materials with heteroatoms such as nitrogen or boron has been reported to enhance hydrogen affinity and increase binding energies, thereby improving low-pressure storage capacities.[40]

Another promising direction involves densification of porous powders into monoliths or pellets without significantly reducing accessible pore volume,[41,42] which can improve volumetric capacity while retaining the gravimetric capacity. In addition, advanced shaping methods, including sol–gel synthesis[43] and 3D printing,[44] have enabled the fabrication of mechanically stable adsorbents with tuned and optimised pore networks.[43]

Molecular simulations, including Grand Canonical Monte Carlo (GCMC) and density functional theory (DFT) calculations,[45] have been pivotal in predicting optimal pore environments and guiding synthetic efforts. By screening large libraries of hypothetical MOFs, computational studies have revealed that the best-performing materials often feature ultramicropores combined with high densities of adsorption sites. Integration of computational design with experimental synthesis is thus a key avenue toward discovering materials that maximise hydrogen density.

It was shown in 2011 that porous materials can also consist of hydrides: a porous magnesium tetrahydridoborate, γ-$Mg(BH_4)_2$, framework has small pores and a unique partially negatively charged non-flat interior capable of reversibly adsorbing small guest molecules such as nitrogen, hydrogen and dichloromethane.[46] More recently, this material was investigated for hydrogen and nitrogen uptake by using neutron powder diffraction, volumetric gas adsorption, inelastic neutron scattering, and first-principles calculations.[47] γ-$Mg(BH_4)_2$ has *ca.* 30% void space in the solid crystal and contains a 3-dimensional network of channels with a pore diameter of ∼9 Å and smaller openings (apertures) of ∼5.8 Å, which enables the adsorption of smaller molecules.[46] This porous substance, γ-$Mg(BH_4)_2$, is distinguished from other porous matter by having a partially negative inner surface formed by $B–H^{\delta-}$–Mg bonds. Surprisingly, ∼3.5 times more hydrogen can be adsorbed in this framework than nitrogen, resulting in the compositions, γ-$Mg(BH_4)_2{\cdot}2.33H_2$ or γ-$Mg(BH_4)_2{\cdot}2/3N_2$.[47] Powder neutron diffraction experiments have revealed extremely dense packing of hydrogen molecules (H_2), which form trigonal bipyramidal units, denoted penta-dihydrogen clusters, $(H_2)_5$, within the channels. This packing structure leads to adsorbed H_2 densities up to ∼144 g H_2 L^{-1} at 25 K, which is about twice that of liquid hydrogen (71 g L^{-1}).[47] This corresponds to 8.0 wt% dihydrogen adsorbed in the porous substance and a total hydrogen content of 21.7 wt%. Furthermore, the first two hydrogen molecules adsorbed in each penta-dihydrogen cluster interact with the solid-state structure *via* non-directional dispersion forces (van der Waals interactions), and these molecules can rotate freely about their centre of mass. This is in contrast to the three following H_2 molecules in the penta-dihydrogen clusters, $(H_2)_5$, which are bound with well-defined directional bonds and are located slightly closer to the lattice structure in porous γ-$Mg(BH_4)_2$. An interaction between molecular hydrogen and the partially negatively charged lattice structure, $B–H^{\delta}—\cdots H_2$, is created. New types of hexa-hydrogen bonds are formed, $(B–H^{\delta}–)_2\cdots H–H\cdots(H^{\delta}––B)_2$, which contribute to the very dense packing of molecular hydrogen.[47] Neutron diffraction reveals that dihydrogen is adsorbed close to the covalently bound hydrogen in the porous host structure (shortest distance, $H\cdots H_2$ of 2.69 Å) and there is a very short distance between the molecules of the penta-dihydrogen units as $H_2\cdots H_2$ of 2.64 Å.[47] This can be compared to solid hydrogen in which the distance between dihydrogen molecules, $H_2\cdots H_2$ is 2.66 Å at a pressure of 5.4 GPa.[48] The high H_2 density in the pores was attributed to the anisotropic shape of the H_2 molecules normally seen at near-ambient pressures as close-packed spheroids. In contrast to hydrogen, nitrogen molecules are located in the middle of a pore, as far from the host structure as possible, whereas hydrogen prefers to be closer to the hydridic apertures. Nitrogen and hydrogen have a similar

kinetic diameter, $d(H_2/D_2)$ = 2.89 Å and $d(N_2)$ = 3.64 Å, which hints towards specific interactions between the negatively charged framework and neutral molecules. Moreover, macroscopic measurements of nitrogen and hydrogen gas adsorption in the porous substance, γ-$Mg(BH_4)_2$, provided very dissimilar results owing to the distinct adsorption sites of these gasses. The calculated Brunauer–Emmett–Teller (BET)-specific surface area for γ-$Mg(BH_4)_2$ determined from an N_2 isotherm measured at 77 K is only $S_{BET}(N_2)$ = 610 $m^2\ g^{-1}$, whereas a H_2 isotherm (measured at 20 K) gives the result $S_{BET}(H_2)$ = 1787 $m^2\ g^{-1}$. This highlights the probe-molecule dependence of BET analysis in small-pore frameworks, where H_2 and N_2 access distinct adsorption sites.[47] Interestingly, larger molecules, such as ethane and noble gasses are capable of entering the pores reversibly, despite having very different kinetics.[49,50]

It was argued that porous γ-$Mg(BH_4)_2$ is the first step towards a new class of nanoporous materials resembling flexible metal–organic frameworks (MOFs).[46] The similarity of these frameworks to MOFs provides a route to novel hybrid materials, where the combined use of tetrahydridoborate complexes, BH_4^-, with other directional ligands may produce new porous materials. This could include materials with a high hydrogen storage density like that demonstrated by γ-$Mg(BH_4)_2$. In particular, the same framework topology is observed for γ-$Mg(BH_4)_2$ and zinc imidazolate framework ZIF-72, and thus prompts the combined use of BH_4^- and imidazolate ions as ligands. Hence, attempts have been made to extend the family of hydridic porous solids by combining imidazolates (ligands known to build stable frameworks) and complex hydrides, yielding hybrid hydrides with unexpected dynamical properties.[51] More complex ligands combining hydridoborates and imidazolates have also been explored.[52]

2.3. Future prospects for porous materials

Currently, porous materials suffer from low storage capacity under ambient conditions and the requirement for expensive cooling or high pressures, poor stability of some materials, particularly after densification or many cycles of hydrogen release and uptake, costs of synthesis and upscaling, low volumetric capacities and system integration challenges, such as low thermal conductivity and compatibility with existing infrastructure.

To improve storage capacity, many MOFs, COFs and PAFs (porous aromatic frameworks) can be tuned to optimise pore size and chemistry, as well as some carbon materials such as carbide-derived carbons, activated and other porous carbons.[53] Techniques such as sol–gel synthesis, hydrothermal synthesis, and chemical vapor deposition,[54] as well as 3D-printing,[44] enable precise pore size distributions. Current research developing adsorbents with enthalpies near the optimal range of ∼−15 to −25 kJ mol^{-1}, which could enable storage under near-ambient conditions, might reduce or eliminate the need for cryogenic cooling. An enthalpy of −21 kJ mol^{-1} for an MOF with exposed vanadium(II) sites has been reported.[55] An imine-based COF with incorporated copper(II) has been found to reversibly adsorb H_2 above room temperature with an enthalpy of hydrogen adsorption of −15 kJ mol^{-1} (ref. 56) and a range of enthalpies from −23 to −33 kJ mol^{-1} have been reported for a Cu-based MOF undergoing post-synthetic modifications with different metals.[57]

Recent advances in continuous-flow synthesis of MOFs,[58] including air–liquid segmented flow[59] and droplet microfluidic systems,[60] as well as new techniques, such as the use of artificial intelligence (AI) and improved packing arrangements;[61] and the use of cheaper, renewable carbon sources, for example, biomass for porous carbons,[62,63] may enable low-cost scalable synthesis. In addition, recent studies of the effects of densification by compaction have indicated that this can result in higher volumetric capacity without structural damage for MOFs such as UiO-66,[42] ZIF-8,[64] and HKUST-1.[43] Repeated cycling of activated carbons[63] and MOFs, such as MOF-5,[65] along with databases and rules and guidelines for MOF design,[66] also shows promise in the design and implementation of materials for long-term cycling.

For large-scale and commercial implementation, thermal management, compact storage and the use of existing hydrogen infrastructure will all need to be addressed. For thermal management, improving the effective thermal conductivity of the absorbent by adding a conductive material, such as graphite[67]/expanded natural graphite (ENG),[68,69] or graphene[70] /graphene oxide,[71] has proven effective, along with advances in the engineering of thermal management systems, such as microchannel cooling plates and liquid nitrogen as a separate cooling fluid.[72] Hybrid approaches may provide further improvements. Hybrid materials, such as $LiBH_4$ in a porous scaffold of carbon wrapped Fe_3O_4,[73] MgH_2 ball-milled with Ni/Fe based MOFs,[74] and MOF-AC hybrids,[75,76] generally provide higher capacity and/or better hydrogen diffusion due to synergistic effects between the two components. Hybrid techniques are also developments that have the potential to facilitate more applications, for example, cryo-adsorption coupled with cryo-compression has the advantages of higher hydrogen capacity than adsorption or compression alone, at a lower pressure than compression and a higher temperature than cryo-compression.[77]

3. Solid-state hydrogen storage

3.1. High hydrogen content hydrides

During the past decade, novel classes of complex hydrides have been reported, some of which have the highest known solid-state gravimetric and volumetric hydrogen densities. This is illustrated by a solid inorganic compound, ammonium tetrahydridoborate, NH_4BH_4, which is isoelectronic to natural gas (CH_4). The two compounds, CH_4 and NH_4BH_4, have similar gravimetric hydrogen densities (∼25 wt% H_2), although NH_4BH_4 has a significantly higher solid-state volumetric density of hydrogen with ρ_V = 157 g L^{-1} (see Table 1). However, NH_4BH_4 is not stable and has a half-life of ∼6 hours owing to slow conversion to the diammoniate of diborane ($[(NH_3)_2BH_2]BH_4$), hydrogen and toxic gases such as ammonia and diborane.[11,12,78]

Table 1 Volumetric, ρ_V, and gravimetric, ρ_m, hydrogen densities of selected hydrogen-rich compounds compared to liquid hydrogen and natural gas (CH_4). Notice that volumetric and gravimetric hydrogen densities are related to the material density, $\rho_V = \rho_m \times \rho$. The approximate decomposition temperature, T_{dec}, is provided for the solids

Compound	ρ_m (wt%)	ρ_V (g L^{-1})	T_{dec} (°C)	Ref.
$H_{2(l)}$	100	71.0	—	86
$CH_{4(l)}$	25.1	106.0	—	86
$MgH_{2(s)}$	7.7	108.7	~330	87
$LiBH_{4(s)}$	18.4	122.5	~400	88
$NH_3BH_{3(s)}$	19.6	143.6	70	79
$NH_4BH_{4(s)}$	24.5	157.0	[a]	11
$NH_4Li(BH_4)_{2(s)}$	22.1	153.1	~52	83
$(NH_4)_3Mg(BH_4)_{5(s)}$	21.1	158.2	~35	83
$(NH_4)_3Mn(BH_4)_{5(s)}$	17.6	154.4	~50	83
$(NH_4)_2Y(BH_4)_5{\cdot}NH_{3(s)}$	17.0	144.3	—	83

[a] Metastable compound.

This is in contrast to the decomposition of ammonia borane, NH_3BH_3, which releases hydrogen through polymerisation *via* polyaminoborane $[NH_2BH_2]_n$ (at 70–100 °C) and polyiminoborane $[NHBH]_n$ (~150 °C) and finally to boron nitride (BN) at temperatures approaching 500 °C.[79] Quasielastic neutron scattering of ammonium tetrahydridoborate, NH_4BH_4, reveals that no reorientation dynamics are present in the low-temperature ordered polymorph at $T < 50$ K (within the timescale 0.1 to 100 ps). However, the ammonium cation is more dynamic than the BH_4^- anions in the high-temperature ($T > 50$ K) disordered polymorph. Initially, NH_4^+ exhibits tetrahedral tumbling, then cubic tumbling towards isotropic rotational motion at increasing temperatures.[80] The highly dynamic structure contributes to the low thermal stability.

Interestingly, it was found that NH_4BH_4 can be stabilised by mechano-chemical reactions with metal tetrahydridoborates, such as $Ca(BH_4)_2$, which forms a perovskite-type compound $NH_4Ca(BH_4)_3$.[81] Ammonium calcium tetrahydridoborate, $NH_4Ca(BH_4)_3$, is the first example of efficient stabilisation of NH_4BH_4 since this compound decomposes to $Ca(BH_4)_2{\cdot}NH_3BH_3$ and hydrogen at $T \sim 100$ °C.[81,82]

A variety of ammonium metal tetrahydridoborates with new compositions and structure types have recently been discovered.[13,83] Full solubility is observed for MBH_4–NH_4BH_4, M = K, Rb, Cs, with formation of solid-solutions, $(NH_4)_xM_{1-x}BH_4$, by cryo-mechano-chemical treatment. The ammonium metal tetrahydridoborates stabilise NH_4BH_4 and suppress the aggressive decomposition and possibly alter the decomposition pathway. However, the thermal stability decreases with increasing ratios of NH_4BH_4 in the compounds owing to increasing numbers of di-hydrogen bonds in the solid-state, facilitating low temperature hydrogen elimination *via* di-hydrogen bonds.[84] The thermal stability of ammonium metal tetrahydridoborates is governed by the Pauling electronegativity of the metal, the structural dimensionality, the dihydrogen bond length, the relative amount of NH_4^+ to BH_4^-, and the nearest coordination sphere of NH_4^+. Hydrogen release of ammonium metal tetrahydridoborates during constant heating often occurs in three steps, involving new intermediate compounds, resulting in crystalline, polymeric, and amorphous materials.[83]

Ammonium metal tetrahydridoborates may have extreme hydrogen densities even if they contain a transition metal (see Table 1). The compound $(NH_4)_3Mn(BH_4)_5$ has an extremely high gravimetric hydrogen content, $\rho_m = 17.6$ wt%, but a record high volumetric hydrogen density, $\rho_V = 154.4$ (g L^{-1}). This latter value is more than twice the density of liquid hydrogen (71.0 g L^{-1}). Ammonium–ammonia hydrido-*closo*-borates, such as $(NH_4)_2B_{10}H_{10}{\cdot}NH_3$ and $(NH_4)_2B_{12}H_{12}{\cdot}NH_3$ have recently received attention due to their potential application as proton conductors.[85] This is owing to the formation of the complex cation, $N_2H_7^+$, that is formed *via* a hydrogen bond between NH_4^+ and NH_3.

However, although these new classes of hydrides possess high hydrogen densities, and often release hydrogen under moderate conditions, their rehydrogenation is not straightforward, and further research efforts are required. Another breakthrough is the discovery of chemical reactions between different hydrides and other compounds, which react to form other compounds during the release of hydrogen that more readily absorb hydrogen during the rehydrogenation process. This research provides new opportunities for the design and tailoring of novel functional materials with interesting properties.

3.2. Hydrogen in high entropy alloys

High entropy alloys (HEAs) are a class of multi-component metallic materials characterised by a high configurational disorder. They are defined as alloys containing five or more elements with an atomic content of between 5 and 35 at%[89] and a mixing entropy larger or equal to 12.5 J mol^{-1} K^{-1}.[90] They offer tuneable thermodynamics and fast hydrogen sorption kinetics. It has been found that, in addition to configurational entropy, other entropic contributions (vibrational, magnetic and electronic entropy), and enthalpies of mixing, could play a significant role in the phase formation and stability of HEAs. This unique composition leads to a complex crystalline structure with a high degree of disorder at the atomic level, which gives HEAs their distinctive properties and makes them potentially suitable for hydrogen storage applications. A key aspect is the myriad of possibilities to customise the composition of these alloys, potentially leading to the development of alloys with excellent hydrogenation properties. In addition, light and inexpensive elements can be incorporated into the compositions, reducing the weight of the alloys along with the cost, and thus increasing the gravimetric hydrogen storage capacity. The literature indicates that, depending on composition and conditions, these alloys can incorporate large amounts of hydrogen into their lattice structure through processes such as interstitial solid solution formation or hydride formation. Due to the increasing number of compositions and complexity, a recent trend in the literature on HEAs is the use of modeling[91] and machine learning (ML)[92] for the prediction and/or optimisation of properties,[93] which can accelerate development and optimisation of such high entropy hydrides.

The studies on HEAs for hydrogen storage focus on three main groups: body-centred cubic (BCC) HEAs, lightweight HEAs and intermetallic HEAs. These groups are related to the traditional hydride-forming metal alloys and are influenced to some extent by the knowledge gained so far. BCC HEAs[94] and intermetallic HEAs[95,96] are named after the crystal structure they form (BCC solid solutions and ordered intermetallic structures). BCC alloys exhibit high hydrogen per metal ratios and can accommodate up to 2 H per M by transforming into fcc structures. Combining ML, DFT calculations and experiments, Agafonov *et al.* successfully optimised the composition of a Ti–V–Nb–Cr–Mo alloy and identified a promising HEA with a capacity of 2.6 wt% and an enthalpy of hydride formation of 38 kJ mol^{-1} H_2.[97] The third group, light HEAs, does not refer to a specific crystal structure, but to the presence of light elements, such as Mg, Al and Li in the HEA structure.[98] Research on lightweight HEAs is mainly focused on improving the gravimetric hydrogen storage capacity by reducing the molar weight of the alloys. Since light HEAs are not bound to a specific crystal structure, they can contain HEAs with BCC, fcc and intermetallic structures. Nevertheless, most of the light HEAs reported so far crystallise in a BCC structure.

Overall, HEAs all have very high volumetric hydrogen density (>100 g H_2 L^{-1}), which is superior to that of liquid H_2, 70 g L^{-1}. They usually also have very fast kinetics for hydrogen release and uptake, and they are considered safe storage media.[99] Furthermore, the gravimetric storage capacity and the thermodynamics for hydrogen release and uptake can be tailored. As an example, the enthalpy of hydride formation for the equimolar alloy $Ti_{25}V_{25}Cr_{25}Nb_{25}$ is $\Delta H = -51.6$ kJ mol^{-1} H_2,[100] whereas that of $Ti_{25}V_{30}Nb_{10}Cr_{31}Mo_4$ is $\Delta H = -40$ kJ mol^{-1} H_2 and this alloy stores 2.24 wt% H_2 reversibly at room temperature.[101]

3.3. Reactive hydride composites for reversible hydrogen storage under moderate conditions

Classical interstitial metal hydrides exhibit favourable volumetric hydrogen storage densities; however, the reversible gravimetric storage capacity under gas-phase loading of such hydrides is typically limited to approximately 2 wt% under practical conditions.[102,103] Such a value is insufficient for most mobile applications. In contrast, Mg-based hydrides such as MgH_2 and Mg_2FeH_6 display significantly higher reversible gravimetric storage capacities of approximately 7 and 5 wt%, respectively.[104,105] Notably, Mg_2FeH_6 possesses one of the highest volumetric storage densities reported, reaching 150 g H_2 L^{-1}.[106] Despite these advantages, Mg-based hydrides suffer from unfavourable thermodynamics as their high hydrogenation enthalpies hinder large-scale implementation, even though kinetic limitations can be partly mitigated through suitable additives.[107,108]

The discovery of reversible hydrogenation in Ti-doped $NaAlH_4$[109] initiated intensive research in the discovery and exploration of numerous new lightweight complex hydrides with markedly improved gravimetric storage densities. $LiBH_4$ has been particularly noteworthy owing to its exceptionally high gravimetric hydrogen content of 18.5 wt%.[110] Unfortunately, both the hydrogenation and dehydrogenation kinetics of such high-capacity complex hydrides remain insufficient for practical use. Partial rehydrogenation of LiH and B to form $LiBH_4$ requires very harsh conditions of 350 bar and 600 °C.[111] To overcome these challenges, Barkhordarian *et al.*[112] demonstrated that rehydrogenation of tetrahydridoborate is considerably more feasible when lightweight hydrides such as LiH, NaH or CaH_2 are combined, for example, with MgB_2 rather than pure B. In such cases, instead of the thermodynamically hindered reaction (1), reaction (2) occurs at significantly lower temperatures and pressures, while reversible dehydrogenation reaction also proceeds under milder conditions. The use of layered MgB_2 instead of icosahedral B plays a key role in facilitating hydrogen uptake and formation of the tetrahydridoborate.[113]

$$xMH_{2/x} + 2B + 3H_2 \rightarrow xM(BH_4)_{2/x} \quad (1)$$

$$xMH_{2/x} + MgB_2 + 4H_2 \rightarrow xM(BH_4)_{2/x} + MgH_2 \quad (2)$$

As early as 2004, enhanced reaction kinetics and thermodynamics in $2LiBH_4/MgH_2$ composites were reported as compared to their single-phase counterparts.[114] Such composites are denoted reactive hydride composites (RHC) and are illustrated in Fig. 3. A critical limitation, however, of such $LiBH_4/MgH_2$ composites remains: the high dehydrogenation temperature of more than 350 °C. Nanoconfinement strategies have since reduced hydrogen release temperatures to below 300 °C.[115,116]

Furthermore, replacing MgH_2 in this composite with the thermodynamically less-stable Mg_2NiH_4 demonstrated a mutual destabilisation effect with $LiBH_4$ lowering the operating temperature to 270 °C, below the melting temperature of $LiBH_4$.[117–119]

Subsequent studies revealed that further optimisation is possible using different types of transition metal-based additives which promote nucleation, maintaining structural integrity of the nanocomposite and thus enabling faster hydrogenation and dehydrogenation kinetics under more moderate conditions.[120,121]

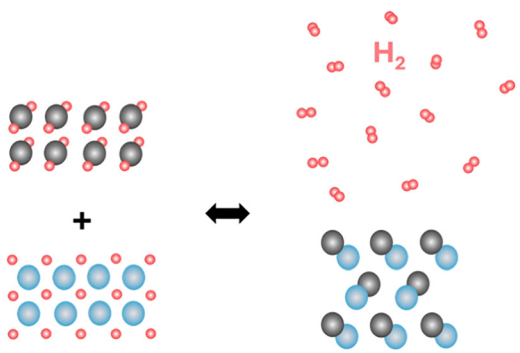

Fig. 3 Illustration of reactive hydride composites (RHC). Initially the hydrides release hydrogen and then react and form a new compound. This new compound may facilitate hydrogen uptake as compared to the individual hydrides.

An alternative destabilisation approach was also reported in 2005.[122] These materials exhibited surprisingly low hydrogen release and uptake temperatures of 170 °C for $Mg(NH_2)_2$/2LiH composites and reasonable reversibility under gas-phase loading. However, the reaction kinetics at 170 °C remained slow, with rehydrogenation times of almost 2 hours. However, the addition of small amounts of $LiBH_4$ dramatically improved kinetics with rehydrogenation occurring within 12 min with the addition of 0.5 mol of $LiBH_4$ to 6 mol $Mg(NH_2)_2$ + 9 mol LiH. Higher amounts of $LiBH_4$ (1 or 2 mol) in this composite lead to shortened rehydrogenation times of 8 min and 4 min, respectively.[123] Further increases in the $LiBH_4$ content accelerated the reaction rates even at near-ambient temperatures. In the $6Mg(NH_2)_2$ + 9LiH + $12LiBH_4$ composite, Wang *et al.* could demonstrate hydrogenation at temperatures as low as 53 °C with a rehydrogenation time of 5 hours at 98 °C.[124] This kinetic destabilisation was accompanied by thermodynamic destabilisation as the equilibrium plateau pressure at 187 °C increased from 20 bar for the binary $6Mg(NH_2)_2$ + 9LiH system to almost 100 bar in the case of the 3-component $6Mg(NH_2)_2$ + 9LiH + $12LiBH_4$ system. Recent work suggests that further optimisation is possible by increasing the $LiBH_4$ content.

Although most complex hydrides suffer from sluggish kinetics at moderate temperatures, these studies highlight the potential of using reacting mixtures of hydrides to tailor both thermodynamic and kinetic properties of lightweight and complex hydride-based materials as a promising alternative strategy for hydrogen storage materials design.

3.4. Solid-state hydrogen storage and transport

Sodium tetrahydridoborate, $NaBH_4$, is a vital reducing agent in numerous organic chemistry syntheses but is also a well-known hydrogen-rich material.[10,125] Over the last 20 years it has been widely investigated for hydrogen storage purposes, but it typically requires high temperatures (>500 °C) for hydrogen release and extreme conditions for rehydrogenation.[126–129] Alternatively, hydrogen release can be obtained from $NaBH_4$ at room temperature using hydrolysis or methanolysis reactions, which were first reported in 1953:[130]

$$NaBH_4 + 2H_2O \rightarrow NaBO_2 + 4H_2 \quad (3)$$

$$NaBH_4 + 4CH_3OH \rightarrow NaB(OCH_3)_4 + 4H_2 \quad (4)$$

The hydrolysis reaction is typically catalysed by metallic nanoparticles for controlled rapid rates of hydrogen gas release.[131–133] The simplicity of sodium borohydride hydrolysis has marked it as a potential hydrogen carrier for energy export.[134] Here, the cost of hydrogen export from Australia to Japan using powdered $NaBH_4$ ($4.40 USD per kg H_2) could be lower than that using ammonia ($5.50 USD per kg H_2), liquid organic hydrogen carriers ($5.90 USD per kg H_2), or liquid hydrogen ($7.10 USD per kg H_2).[134] These costs include the renewable production of the hydrogen and the carrier, along with transport and reconversion costs. Another cost-efficient aspect of the process is that the thermodynamics for the hydrolysis and methanolysis suggest that high hydrogen pressure is possible, and it has been demonstrated that up to 1000 bar H_2 has been generated, which is comparable to mechanical compression technology.[134]

If $NaBH_4$ is to become a hydrogen export material, a green, low-cost regeneration method from the $NaBO_2$ hydrolysis product to $NaBH_4$ must be realised. This excludes the typical synthesis method using the Brown–Schlesinger or Bayer processes, as the starting materials are $B(OCH_3)_3$ and $Na_2B_4O_7 \cdot 7SiO_2$, respectively.[135] Since 2003, regeneration using thermochemical, mechano-chemical and electrochemical techniques has been demonstrated.[132,136] The highest yields have been achieved using magnesium or magnesium hydride as a reactant with the formation of MgO, although Si, Al, $Mg_{17}Al_{12}$, Mg_2Si, Na_2CO_3 and other additives have also been reported.[136,137] For the thermochemical method, temperature is the main barrier in the process, with 600 °C at a H_2 pressure of 70 bar being required to achieve a 97% yield,[138] although a H_2 pressure of 21 bar at 600 °C has also shown to be effective to achieve 90% conversion.[139] Mechano-chemistry at room temperature under an argon or hydrogen atmosphere can also achieve high yields, but long milling times are required.[136] This method may also suffer from scale up issues due to the ball to powder ratio required and limited size of mills. Electrochemistry processes are carried out in an electrochemical cell which consists of an anode and a cathode according to eqn (5) and (6) below:

$$\text{Cathode: } BO_2^- + 6H_2O + 8e^- \rightarrow BO_4^- + 8OH^- \quad (5)$$

$$\text{Anode: } 8OH^- \rightarrow 4H_2O + 2O_2 + 8e^- \quad (6)$$

There have been several publications on the electrochemical synthesis of $NaBH_4$ using various electrolytes, membranes and electrodes, but replication of these data has been reported to be difficult.[136,140] One important aspect to overcome is preventing the decomposition of water into hydrogen and oxygen, while at the same time improving electron efficiency to reduce costs. Once the cost-effective synthesis of $NaBH_4$ has been achieved, the extraction of the $NaBH_4$ powder from residual $NaBO_2$ must also be optimised given their similar solubilities in water and general insolubility in aprotic solvents.[141,142]

4. Solid-state battery materials, hydrides as electrolytes

4.1. Overview

Traditional oxides and halides often have close-packed structures and only have cationic conductivity at very high temperatures owing to defect formation. New classes of hydridoborate-based materials have been discovered during the past decade, which have more open and flexible structures. These hydrides provide new routes to create fast cationic conducting materials as functional solid-state battery materials. Simultaneously, it has become clear that several new phenomena in the solid-state can enhance the ionic conductivity for this class of materials. Impressively, this can lead to novel fast cationic conductivity of divalent cations at moderate temperatures ($T < 100$ °C).

Lithium tetrahydridoborate was recognised as a fast lithium ionic conducting material in 2007, but only at $T > \sim 110$ °C, owing to a polymorphic transition forming the disordered high temperature variant, h-$LiBH_4$ (with a hexagonal structure).[143] This polymorph can be stabilised at room temperature by anion substitution resulting in the formation of solid solutions, $LiBH_4$–LiX, X = Cl, Br, I, reaching high Li^+ conductivities. The high conductivity was assigned to anionic dynamics in the solid-state.[144]

4.2. Hydroborate-based magnesium electrolytes

An ammonia derivative of magnesium tetrahydridoborate, $Mg(BH_4)_2{\cdot}NH_3$, was discovered recently, with a relatively open structure consisting of one-dimensional zig-zag chains of –BH_4–Mg–BH_4–Mg– running along the *b*-axis with one terminal and two bridging BH_4^- complexes. The chains are interlinked by dihydrogen bonds, $B–H^{\delta-}\cdots{}^{+\delta}H–N$, created by partly positively charged hydrogen bonded to nitrogen and partly negatively charged hydrogen atoms bonded to boron. Dihydrogen bonds are the inorganic analogue to hydrogen bonds found in most biological matter with the same bond length (~2 Å) and strength (~20 kJ mol^{-1}).[17] The monoamine, $Mg(BH_4)_2{\cdot}NH_3$, derivative of the series of compounds, $Mg(BH_4)_2{\cdot}xNH_3$, x = 0, 1, 2, 3, 6, has the highest Mg^{2+} conductivity, $\sigma(Mg^{2+})$ = 3.3 × 10^{-4} S cm^{-1} at 80 °C, which is approximately 8 orders of magnitude higher than that of $Mg(BH_4)_2$.[145]

DFT calculations reveal that the fast cationic conductivity is owing to the weak di-hydrogen interactions, flexible coordination of the BH_4^- complex, and exchange of the neutral molecule, ammonia (NH_3), between interstitial and framework magnesium. This is considered a new mechanism for cationic conductivity denoted 'ligand-assisted cationic conductivity', which is unique for hydridoborate-based electrolytes.[17]

Surprisingly, mixing any two compounds in the series, $Mg(BH_4)_2{\cdot}xNH_3$, x = 0, 1, 2, 3, 6, increases the conductivity by one to three orders of magnitude. In addition, the composite $0.4Mg(BH_4)_2{\cdot}NH_3$–$0.6Mg(BH_4)_2{\cdot}2NH_3$, has a rather low eutectic melting point ($T \sim 55$ °C). Also, the addition of larger amounts of inert, insulating nanoparticles, *e.g.* Al_2O_3 (~75 wt%), stabilises the molten phase to become a solid at room temperature.[145] Micrographs show that the molten phase is distributed over the nanoparticles as a surface layer, but the dynamic properties of the molten state are preserved providing high conductivity at low temperatures, *e.g.* $\sigma(Mg^{2+}) \sim 2.5 \times 10^{-5}$ S cm^{-1} at T = 22 °C for the composite, $0.4Mg(BH_4)_2{\cdot}NH_3$–$0.6Mg(BH_4)_2{\cdot}2NH_3$–$Al_2O_3$, denoted $Mg(BH_4)_2{\cdot}1.6NH_3$–Al_2O_3.[146] This phenomenon also increases the conductivity of divalent cations, at low temperatures, which is otherwise very difficult to achieve. These nanocomposites exhibit good mechanical and thermal stability and benefit from nanoconfinement strategies that preserve interfacial dynamics and enhance divalent-ion transport. A nanocomposite material was recently demonstrated as a functional electrolyte for an inorganic solid-state magnesium battery using Mg-metal as the anode, layered titanium disulfide (TiS_2) as an intercalation cathode, and a nanocomposite as electrolyte, $Mg(BH_4)_2{\cdot}1.6NH_3$–MgO (75 wt%).[147]

Multiple derivatives of magnesium tetrahydridoborate have been investigated recently containing neutral molecules, which can introduce weak interactions (dispersion/van der Waals) between apolar molecular moieties along with dihydrogen bonds between partly positive and partly negative hydrogen atoms. A series of new compounds have been discovered, *e.g.* $Mg(BH_4)_2{\cdot}xCH_3NH_2$, x = 1, 3, 6,[148] $Mg(BH_4)_2{\cdot}x(CH_2)_4O$, x = 0, 2/3, 2, and 3 ($(CH_2)_4O$, tetrahydrofuran, THF),[149] and $Mg(BH_4)_2{\cdot}x(CH_3)_2CHNH_2$, x = 1, 2, 3 (isopropylamine, IPA).[150] It has been noted that compounds with layered (two-dimensional) or chain-like (one-dimensional) structures often have the highest cationic conductivity. The structures of these materials are dominated by polar covalent bonding explaining their extremely low electronic conductivity ($\sigma_e < 10^{-12}$ S cm^{-1} at RT). The weak bonding introduces structural flexibility, which promotes record high conductivity of divalent cations, *e.g.* $\sigma(Mg^{2+}) \sim 1.5 \times 10^{-4}$ S cm^{-1} at RT of β-$Mg(BH_4)_2{\cdot}CH_3NH_2$ (Fig. 4).[148] Metal tetrahydridoborates also have very high ionic selectivity, *i.e.* only one type of ion is mobile in the material, observed as very high cationic transport numbers ($t_+ \sim 1$).

The nanocomposite, $Mg(BH_4)_2{\cdot}1.5THF$–MgO, displayed very high conductivity, $\sigma(Mg^{2+}) \sim 10^{-4}$ S cm^{-1} at 70 °C, and a high ionic transport number of t_+ = 0.99, and cyclic voltammetry revealed an oxidative stability of ~1.2 V *vs.* Mg^{2+}/Mg.[149] The electrolyte was stable towards magnesium electrodes, which allowed for stable Mg plating/stripping for at least 100 cycles at 55 °C. The first rechargeable inorganic all-solid-state magnesium battery was presented using this electrolyte: Mg | $Mg(BH_4)_2{\cdot}1.5THF$–MgO | Mg_yTiS_2.[149] These new derivatives of magnesium tetrahydridoborate display the highest Mg^{2+} cationic conductivities at moderate temperatures among all known solids and have an extremely large structural and compositional diversity and offer continued possibilities for the discovery of new compounds.[1]

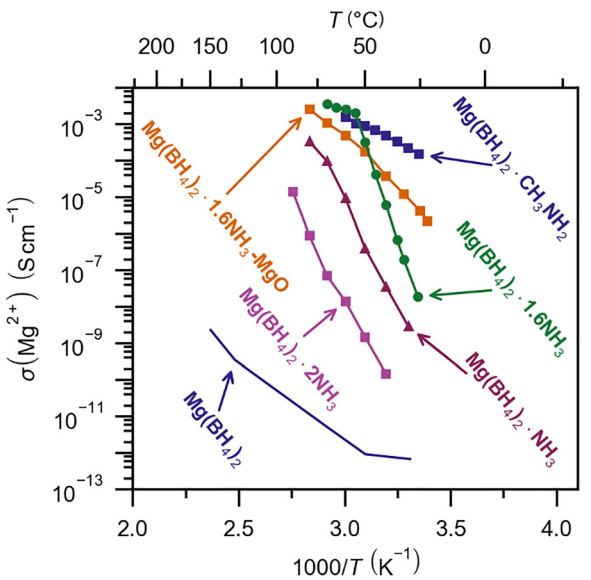

Fig. 4 Magnesium ionic conductivity as a function of temperature for derivatives of magnesium tetrahydridoborate. Raw data presented in Fig. 4 are published in ref. 17, 145 and 148.

Several derivatives of lithium tetrahydridoborate have also been investigated, such as $LiBH_4{\cdot}0.5NH_3$ and $LiBH_4{\cdot}CH_3NH_2$, with fast Li^+ ionic conductivity.[151] A nanocomposite $LiBH_4{\cdot}0.5NH_3$–Li_2O–Al_2O_3, achieved a high conductivity of $\sigma(Li^+)$ = 1.1 × 10^{-3} S cm^{-1} at T = 30 °C.[152,153] A new solid-state rechargeable lithium battery was assembled, Li | $LiBH_4{\cdot}CH_3NH_2$ | TiS_2 (battery voltage 2.1 V), based on a $LiBH_4{\cdot}CH_3NH_2$ electrolyte with a conductivity of $\sigma(Li^+)$ = 1.24 × 10^{-4} S cm^{-1} at RT.[154]

However, the most remarkable findings are the extremely high calcium cationic conductivity of some derivatives of calcium tetrahydridoborates, which are approaching the relevant values of solid state batteries. A series of urea calcium tetrahydridoborates were recently discovered, $Ca(BH_4)_2{\cdot}xCO(NH_2)_2$, x = 2, 4, and 6. The highest cationic conductivity is observed for a composite with average composition $Ca(BH_4)_2$–$6.52CO(NH_2)_2$, $\sigma(Ca^{2+})$ = 1.23 × 10^{-4} S cm^{-1} at 70 °C.[155] A series of crystalline methylamine calcium tetrahydridoborates, $Ca(BH_4)_2{\cdot}xCH_3NH_2$, x = 1, 2, 4, 6 were also discovered. The compound $Ca(BH_4)_2{\cdot}2NH_2CH_3$ has a conductivity of $\sigma(Ca^{2+})$ ~ 10^{-5} S cm^{-1} at T = 70 °C and high ionic transport number close to unity, t_{ion} = 0.9916. This is assigned to a relatively open and flexible octahedral structure built from layers of $[Ca(NH_2CH_3)_2(BH_4)_4]$ complexes in a *cis*-geometry, connected by apolar moieties and weak dihydrogen bonds. An electrochemical cell demonstrated plating and stripping of calcium.[156] Although thermal stability generally decreases with increasing CH_3NH_2 content, the mechanical and thermal stability was increased for nanocomposites, which also showed an increase in the ionic conductivity, *e.g.* $Ca(BH_4)_2{\cdot}4CH_3NH_2$–MgO (50 wt%), $\sigma(Ca^{2+})$ = 1.3 × 10^{-4} S cm^{-1} at 60 °C.[157] These studies indicate that higher calcium ionic conductivities are observed for derivatives with a higher content of neutral molecules, in contrast to magnesium tetrahydridoborate derivatives (Fig. 5).

4.3. *Closo*-Borates as electrolytes

Early studies focussed on derivatives of tetrahydridoborate (BH_4^-) systems as described above, but research has recently shifted towards the use of *closo*-decaborates ($B_{10}H_{10}^{2-}$) and *closo*-dodecaborates ($B_{12}H_{12}^{2-}$) (Fig. 6). The larger *closo*-borates and *closo*-carbaborates have polymorphic order/disorder transitions from low-temperature (LT) ordered to high-temperature (HT) disordered structures. These transitions are related to dynamics of the anion lattice, *i.e.* rotation, reorientation and/or vibration of anions. This motion in the anion lattice can be correlated with cation migration, denoted the 'paddle-wheel' mechanism, which is often observed as the step-wise increase of cationic conductivity.[158,159]

The interest in metal *closo*-borates as electrolytes was initiated by the investigation of $Li_2B_{12}H_{12}$ with significant anion disorder in the high temperature polymorph.[160,161] Moreover, the large composite borate anions have a low charge, typically −1 or −2, which provides a low charge density and weaker interaction with cations.[162] A recent study demonstrated that introducing strain and/or defects into the $Li_2B_{12}H_{12}$ crystal lattice by ball milling can improve ionic conductivity, while partial thermal decomposition at 380 °C leads to an increase in Li^+ conductivity by ~ 2 orders of magnitude compared to the pristine material ($\sigma(Li^+)$ = 1.03 × 10^{-6} S cm^{-1} at 30 °C and $\sigma(Li^+)$ = 1.74 × 10^{-8} S cm^{-1}, respectively).[163] Future work on modifications of these *closo*-borates could improve their ionic conductivity and electrochemical stability as solid-state electrolytes.

The direct synthesis of double anion *closo*-borates, such as $Na_4(B_{12}H_{12})(B_{10}H_{10})$, has also been successfully used for the formation of functional electrolytes with fast sodium conductivity of $\sigma(Na^+)$ ~ 1 mS cm^{-1} at 25 °C.[164] Related advances in solid electrolytes have enabled anode-free all-solid-state sodium batteries with stable cycling, underscoring the relevance of hydride-based electrolytes for next-generation architectures.[165]

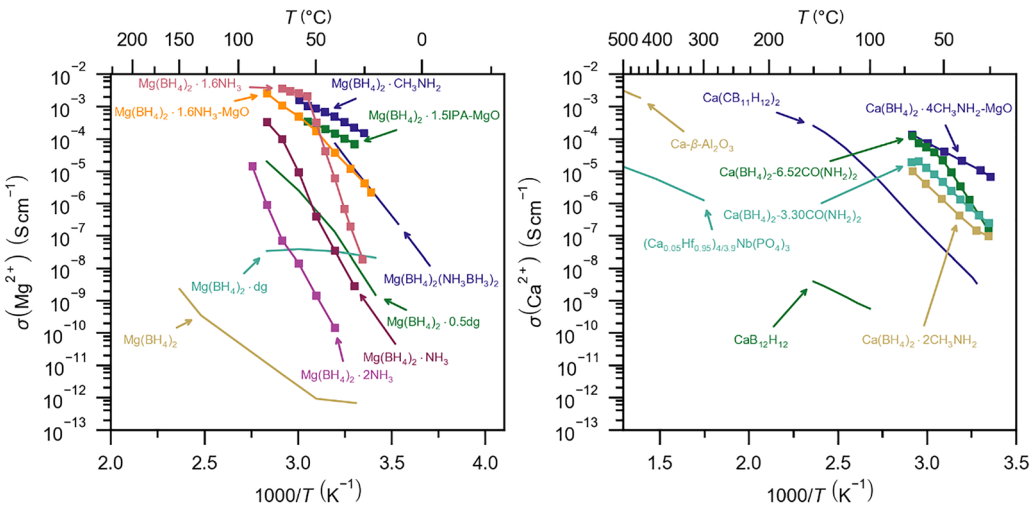

Fig. 5 Calcium ionic conductivity as a function of temperature for derivatives of calcium tetrahydridoborate compared to that of known oxide, phosphate and hydrido-*closo*-(carba)borate based electrolytes. Raw data presented in Fig. 5 are published in ref. 155–157.

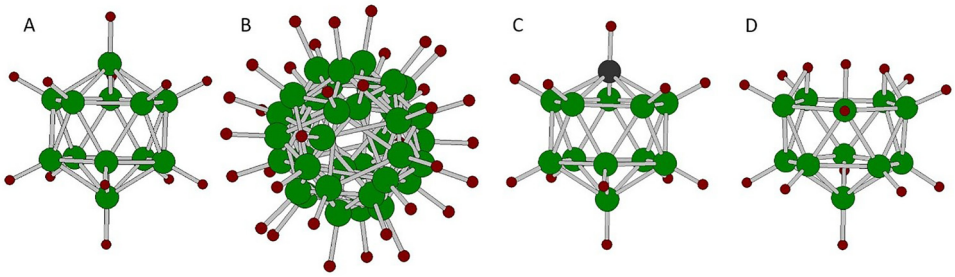

Fig. 6 Structure of selected hydridoborate anions. (A) Dodecahydrido-*closo*-dodecaborate(2−) anion, $B_{12}H_{12}^{2-}$, in an ordered structure. (B) Dodecahydrido-*closo*-dodecaborates anion, $B_{12}H_{12}^{2-}$, in a disordered structure where the anion is statistically or dynamically distributed over two crystallographic positions. (C) Dodecahydrido-*closo*-monocarbadodecaborate(1−), $CB_{11}H_{12}^{-}$. (D) Tetradecahydrido-*nido*-undecaborate(1−), $B_{11}H_{14}^{-}$.

Over the past few decades, it has been shown that these higher borates have large structural flexibility and can provide high ionic conductivities. Further insights allowed for investigations of monovalent *closo*-carbaborates (*e.g.* $CB_{11}H_{12}^{-}$) and *nido*-borates (*e.g.* $B_{11}H_{14}^{-}$), which were potentially more weakly coordinated to cations due to their weaker anionic charge.

4.4. Nido-borates as electrolytes

Alkali-$B_{11}H_{14}$ salts can be conveniently prepared from $NaBH_4$ *via* a single step low-cost reaction.[166] The hydrated $LiB_{11}H_{14}$ and $NaB_{11}H_{14}$ salts display high RT ionic conductivities near 1×10^{-4} S cm^{-1} and 1×10^{-3} S cm^{-1}, respectively. Similar to the *closo*-carbadodecaborates, thermal decomposition results in hydroxylation of the anion, but even in the hydrated state the salts present an oxidative stability above 2 V *vs.* Li^+/Li.[166] Interestingly, $LiB_{11}H_{14}{\cdot}2H_2O$ is an ionic liquid that melts at 70 °C and can be used as a liquid electrolyte.[167] If water is removed from the material, resulting in $LiB_{11}H_{14}{\cdot}(H_2O)_n$ ($n < 2$), it remains solid at these temperatures, but exhibits an enhanced ionic conductivity of 3.2×10^{-2} S cm^{-1}.[167] Hybrid solid–liquid battery cells made from $LiB_{11}H_{14}$ composites show impressive cycling with a TiS_2 cathode and metallic Li anode due to improved SSE/Li contact.[167] Analogous to the $B_{11}H_{14}^{-}$ anion is the divalent $B_{11}H_{13}^{2-}$, where $Na_2B_{11}H_{13}$ shows a similar ionic conductivity to that of the corresponding *closo*-carbadodecaborate, but lower than that of $NaB_{11}H_{14}$.[168] The ionic conductivity of $Na_2B_{11}H_{13}$ is improved at room temperature to almost 1×10^{-4} S cm^{-1} through anionic mixing to form $Na_{11}(B_{11}H_{14})_3(B_{11}H_{13})_4$, which is a higher ionic conductivity than that of hydrated $NaB_{11}H_{14}$.[168]

4.5. Derivatives of higher borates as electrolytes

$CB_{11}H_{12}^{-}$ is a carbon-substituted *closo*-dodecaborate anion. Other substitutions can also be used as weakly coordinating anions to form interesting derivatives. For example, the terminal hydrogen atom, B–H unit in $B_{12}H_{12}^{2-}$, can be substituted by a heavy metal atom, such as Pb, to form a $B_{11}H_{11}Pb^{2-}$ anion. $Li_2B_{11}H_{11}Pb{\cdot}xH_2O$ shows ionic conductivities of up to 7 mS cm^{-1} at 120 °C and an oxidative stability of 2.3 V *vs.* Li^+/Li.[169] Substitution can also be undertaken with Sn, where $Li_2B_{11}H_{11}Sn$ shows an ionic conductivity of 8 mS cm^{-1} at 130 °C and similar oxidative stability.[170] Alternatively, instead of substituting a B–H unit, one can substitute a single H atom on the $B_{12}H_{12}^{2-}$ anion with an ammonia group to form the monovalent $B_{12}H_{11}NH_3^{-}$ anion. Structural similarities exist between $Na_2B_{12}H_{12}$ and $NaB_{12}H_{11}NH_3$ with high temperature polymorphic phase transitions resulting in the ionic conductivity of both Li and $NaB_{12}H_{11}NH_3$ above 1×10^{-4} S cm^{-1} at 200 °C.[171] These ionic conductivities far exceed those displayed by other derivatives such as the class of alkali metal $B_{12}(OH)_{12}^{2-}$ compounds ($< 1 \times 10^{-4}$ S cm^{-1} at 250 °C) or the halogenated variants, $B_{12}X_{12}^{2-}$, where X = Cl, Br, or I, which only reach high ionic conductivity (0.1 S cm^{-1}) at 500 °C.[172,173] It is not only the *closo*-borates that display interesting structural properties and ionic conductivities. The alkali alkoxyborates also show interesting ionic conductivities approaching 1×10^{-2} S cm^{-1} below 200 °C, which may offer cheaper options for future research studies that approach industrial requirements for cost and scalability.[174]

4.6. Borates in organic liquid or polymeric matrix as electrolytes

To date, the majority of ion conductor research, with respect to boron-based hydrides, has been in the solid-state. However, an increasing amount of research has focused on the electrochemical properties of boron-based hydrides in organic solvents and polymer composites. The unique ability of boron-based hydrides to function as ion conductors in the pure solid-state, solution, and composites sets them apart from the other classes of electrolytes currently used in commercial batteries ($LiPF_6$, $LiClO_4$, $LiN(SO_2CF_3)_2$) and those investigated for solid-state batteries (oxides, sulphides, and halides). This feature could enable the rational design and tailoring of the hydroborate electrolyte system for specific applications (*i.e.* vehicular, stationary, extreme conditions). The majority of research using hydroborate in liquid electrolytes has focused on divalent battery chemistries such as Mg^{2+} and Ca^{2+}, while there are very few studies on Li^+.[175,176] The early seminal work of Mohtadi using $Mg(BH_4)_2$ as a liquid electrolyte in a Mg/Mo_6S_8 cell highlighted the importance of solvent selection and additives such as $LiBH_4$ to achieve favourable electrochemical properties.[177] Subsequent work evaluated the impact of various solvent systems and additives such as ionic liquids, glymes, and crown ethers on the electrochemical, solvation dynamics, and interface properties.[178–183] The reactive nature of the BH_4^{-},

and incompatibility with high-voltage cathodes, led to the emergence of the magnesium monocarbaborate (MMC) electrolyte, *e.g.* $Mg(CB_{11}H_{12})_2$ in tetraglyme.[184–186] Using the MMC dissolved in diglyme or tetraglyme as the liquid electrolyte, a highly stable and efficient battery with a high-voltage organic cathode was recently demonstrated.[187] The development of calcium ion batteries has lagged behind that of magnesium given the first demonstration of reversible electrochemical plating and stripping of calcium was reported in 2018 for a $Ca(BH_4)_2$–THF liquid electrolyte.[188] The interphase formation/evolution and solvation environment have also been evaluated at the molecular level.[189–191] Mirroring the development of magnesium liquid electrolytes, the use of a calcium monocarborane (CMC) in a THF/DME solvent mixture facilitated the charge and discharge of a Ca/S battery.[192]

The development of gel polymer and free-standing polymer electrolytes utilising boron hydrides has also been recently investigated. The use of polymer electrolytes could improve the energy density and reduce the interfacial resistance that often plagues many solid-state electrolytes. This could also help reduce the quantity of boron-hydride needed for a battery and allow for the use of tape casting for the electrolyte layer during cell assembly. Both advantages could lead to a significant reduction in the cost of battery manufacturing if commercialised. Free standing polyethylene oxide (PEO) based polymer electrolyte films have been demonstrated using $Mg(BH_4)_2$ and $LiBH_4$.[193–195] However, the ionic conductivity at or near room temperature is relatively low ($<10^{-5}$ S cm^{-1}) requiring the addition of heat to increase the conductivity and to facilitate reversible cation insertion/extraction with a cathode. To overcome these issues, recent work has turned to gel polymer electrolytes (GPE) which incorporate a plasticiser into the polymer and can achieve high ionic conduction at room temperature ($>10^{-4}$ S cm^{-1}) and reduced interfacial resistance. GPEs have been developed by incorporating $Ca(BH_4)_2$, $Mg(BH_4)_2$, $LiBH_4$, or $Li_2B_{12}H_{12}$ into polymers such as PVDF, *p*-THF, and PMMA.[196–200] These GPEs have shown the ability to allow battery cycling at or below room temperature and to prepare flexible batteries. Recent work has also demonstrated that it is possible to anchor and immobilise lithium monocarborane on a polymer to form liquid crystal electrolytes which could lead to new opportunities for future electrolyte designs and opportunities.[201,202]

5. Hydrides as superconductors

Since the theoretical prediction of metallic hydrogen in 1935 and the subsequent prediction of it possessing superconductivity at or near room temperature, an ongoing quest has been undertaken to create this still elusive state of hydrogen.[203,204] The concept of hydrogen ''precompression'', through the use of metal hydrides, represented a possible avenue to overcome the extreme pressures needed to achieve the density of metallic hydrogen in materials under experimentally achievable pressures.[205] This concept led to the prediction of stable hydrogen clathrate-like structures composed of weakly covalent bonding hydrogen atoms with a lanthanide (Ln) atom at the centre of the hydrogen cage.[206] These structures were predicted to possess critical superconducting transition temperatures (T_c) approaching room temperature. However, these structures are only stable at pressures $>$ 100 GPa requiring the use of diamond anvil cell (DAC) conditions. This theoretical prediction was then confirmed experimentally through the observation of superconductivity in a LaH_{10} species at 250 K under 150 GPa of pressure.[207] Since this report, a number of other binary lanthanide hydride phases with T_c values greater than 100 K (YH_9 at 243 K and 201 GPa,[208] CeH_9 at 115 K and 95 GPa,[209] and ThH_{10} at 159 K and 174 GPa[210]) have been shown to be stable and display behaviour consistent with superconductivity (*i.e.* resistance, $R = 0\ \Omega$ below the T_c). These clathrate-like phases of lanthanide hydrides significantly exceed the expected stoichiometry of typical lanthanide hydrides (LnH_x, $x \leq 3$) that can be readily achieved at pressures available from commercial hydrogen gas cylinders.

Non-lanthanide hydride species have been experimentally verified as possessing properties consistent with superconductivity, such as CaH_6 at 210 K and 160 GPa,[211] H_3S at 260 K and 160 GPa,[212] and SnH_x at 70 K and 200 GPa.[213] Much like the lanthanide hydrides, these species also possess a metal to hydrogen stoichiometry that exceeds what would be expected for stable ambient pressure hydrides for these metals (*i.e.* CaH_2 and SnH_4). Alloys and multi-element hydrides have also been experimentally confirmed to behave like superconductors with notable examples including $(La,Ce)H_9$ at 176 K and 100 GPa,[214] $(Y,Ce)H_9$ at 131 K and 114 GPa,[215] $(La,Y)H_{10}$ at 253 K and 183 GPa,[216] and $(LaCeY)H_{10}$ at 190 K and 112 GPa.[217]

Superconductivity in these materials is attributed to the contribution of high electronic densities of states at the Fermi level and strong electron–phonon coupling due to the high density of hydrogen, with some reports consistent with Bardeen–Cooper–Schrieffer (BCS) superconductivity theory.[218] While the results on superconductivity in metal hydrides have led to the rapid expansion of this field, there are some who call into question these results and make counter arguments for these materials not being superconductive at all.[219,220] This stems from the recent retraction of many high profile superconductivity claims, accusations of academic fraud, lack of reproducible results on such small sample sizes (typically on the microgram scale), and difficulty in measuring other hallmarks of superconductivity like the Meissner Effect in DAC on extremely small samples.[221] This opens the door for further advancement in this field by developing advanced measurement techniques or devising new strategies to stabilise hydride superconductors and similar high-pressure phases for characterisation near ambient pressure. For example, recent theoretical predictions suggest that certain perovskite hydrides (ABH_3) can be superconductive between 140 and 170 K below 10 GPa, while ternary hydrides such as a metastable Mg_2IrH_6 may be superconductive at 160 K at ambient pressure.[222,223] Also, partial hole doping of $Ca(BH_4)_2$ through replacement of Ca with K in the structure could potentially achieve ambient

pressure superconductivity at 110 K.[224] In addition, recent studies have also demonstrated that nanosizing and nonconfinement of lanthanide hydrides could stabilise higher order hydrides at pressures much lower than the bulk lanthanide hydride.[225,226] Most recently, it was predicted that Al substituted Mg_2FeH_6 hydride could exhibit superconductivity at a critical temperature of about 130 K under ambient pressure conditions.[227] This finding provides a promising pathway toward the development of practical high-temperature superconductors.

6. New approaches to hydride synthesis

6.1. Overview

Mechanochemical techniques, *e.g.* ball milling, are widely used in various scientific fields, particularly in synthesising solid-state hydrogen storage materials.[228] Despite significant advantages, historically, mechanochemistry has been associated with several limitations such as imprecise control over reaction conditions (*e.g.*, temperature and energy input),[229] leading to inconsistent outcomes and scalability issues. In addition, the fundamental mechanisms behind mechanochemical reactions were poorly understood, causing debate about the reliability and reproducibility of the results. However, monitoring the mechanochemical synthesis by *in situ* powder X-ray diffraction can reveal unexpected insight into the reaction mechanism such as short-lived, metastable intermediates, as observed in the synthesis of metal-organic framework ZIF-8.[230] Advances in mill design now allow controlled temperature and pressure environments, while the development of *in situ* and *operando* diagnostic techniques (*e.g.* X-ray diffraction, Raman spectroscopy and calorimetry during milling) has significantly improved insight into reaction pathways and kinetics.[231]

Recent advancements have shown that combining mechanochemical processes with other energy sources, such as light (photo-mechanochemistry), sound (sono-mechanochemistry), electrical fields or impulses (electro-mechanochemistry), and heat (thermo-mechanochemistry), can overcome traditional activation energy barriers and show promise for the synthesis of hydrogen storage materials.[232] These hybrid approaches enhance control over reaction conditions, enable novel reactions, increase reaction rates and selectivity, and allow for the synthesis of products that are not achievable through conventional mechanochemical methods alone. As a result, these hybrid techniques can overcome traditional barriers[233] and are becoming useful in the field of hydrogen storage materials. Alternatively, a counterintuitive way of performing mechanically induced reactions with theoretically very low energies (without using grinding media) has also gained popularity and can produce contamination-free products with yields higher than those of classical methods.[234–236] Mechanochemistry also provides a way to eliminate the need for bulk solvents used in organic synthesis and can reduce both contamination and the generation of waste. Mechanochemistry approaches can enable different reaction mechanisms and thereby new strategies for synthesis and reaction products not readily accessible by solution based methods.[237]

6.2. High-temperature reactive milling

High-temperature reactive milling (HTRM) was among the first methods used for synthesising magnesium hydride, MgH_2. In 1961, Dymova *et al.*[238] used a rotating stainless steel autoclave in a furnace to synthesise MgH_2 with a 97–98% yield, using iodine as a catalyst and solved issues previously observed by Wiberg *et al.*[239] Huot *et al.*[240] introduced a high-temperature milling method under hydrogen with the addition of graphite. This significantly accelerated the initial hydrogenation process of magnesium, achieving complete hydrogenation in about one hour. This method combined high temperature (300 °C), hydrogen pressure (4 bar), and graphite additives to enhance the synthesis efficiency and hydrogen sorption properties of magnesium hydride. Recently, Baran *et al.* proposed an original method using a high-energy planetary ball mill redesigned to control temperatures up to 450 °C and hydrogen pressure up to 100 bar.[15] They synthesised magnesium hydride under controlled conditions, finding that higher temperatures enhance reaction rates and yields. However, they found that applying the same technique to synthesise ternary hydrides, such as Mg_2FeH_6, Mg_2NiH_4 or Mg_2CoH_5, encountered issues such as an agglomeration of transition metals, requiring further optimization of milling parameters and experimenting with different (more brittle) materials.[241–243]

6.3. Low-energy reactive milling

Despite the advantages that ball milling provides (*i.e.* high stress and strain in reactant particles), it can also result in significant introduction of contamination, uncontrolled phase transformations, and local overheating. This variability has led to the development of low-energy mechanochemical approaches without grinding media. For instance, Pistidda *et al.* investigated the hydrogenation of magnesium diboride, MgB_2, using low-energy milling, showing that particle collisions were sufficient to facilitate the reduction of crystallite size, increase lattice strain, and cause hydrogen uptake of 2.1 wt% using operating parameters of 550 rpm for 50 h.[234] Patel *et al.* applied a similar approach to solve the difficulties of activation of intermetallic FeTi.[235] Room temperature activation was demonstrated without modification of FeTi by alloying elements[244] or heat treatment, with a near theoretical hydrogen capacity being achieved (1.8 wt%). Wyrebska *et al.* demonstrated the spontaneous room temperature reaction of titanium, and its alloys, with hydrogen during self-shearing reactive milling.[236] Using this cost-effective method, titanium hydride was synthesised at close to a 100% yield. These studies highlight the potential of low-energy mechanochemistry in synthesising advanced hydrogen storage materials under moderate conditions, achieving contamination-free and cost-effective synthesis of various hydrogen storage materials.

7. Conclusions and outlook

Hydrogen-based materials show highly interesting and promising properties for a wide range of energy-related applications including hydrogen storage and compression, electrochemical energy storage and superconductivity.

Nanoporous materials such as carbons, MOFs, COFs, and hydride-based frameworks remain potential hydrogen storage materials, due to their tuneable pore structures and high surface areas, as well as good reversibility at moderate pressures. However, practical or commercial implementation is limited by the low adsorption enthalpies which require cryogenic conditions, low volumetric capacities, high synthesis costs, and poor structural stability with cycling. Despite this, progress in tuning pore size distributions, introducing functional groups, doping, densification, and forming hybrid or composite materials has advanced the scope of applications.

Hydrides offer the advantage of high volumetric hydrogen storage density and safe hydrogen storage even under ambient conditions and are also suitable for long time storage. Challenges remain to improve either the thermodynamics or kinetics, and reversibility of those hydrides that show the highest gravimetric storage densities. However, new approaches have been shown both to improve the key properties of hydrogen rich materials for hydrogen storage and to design completely new classes of materials and/or modify the mechanisms for hydrogen uptake and release.

New synthesis techniques, scalable processing, and improved thermal management strategies have the possibility of reducing costs, and computational modelling and AI provide inspiration for future avenues for development of optimised materials. Furthermore, theoretical approaches may also help to discover novel super-hydrides with unexpected, extremely high hydrogen contents, which may be superconducting at temperatures approaching ambient conditions.

Generally, many solid-state hydridoborates have been found to have extremely high cationic conductivity, both for monovalent cations, such as Li^+, Na^+, K^+ or Ag^+, and remarkably also for divalent cations, *e.g.* Mg^{2+} or Ca^{2+}. They also have ionic transport numbers close to one ($t_+ \sim 1$), which contrasts with polymeric and liquid electrolytes ($t_+ \sim 0.5$).[245] Solid state hydridoborate electrolytes also reveal very high charge carrier selectivity with no indication of any H^+, H^- or anion mobility and extremely low electronic conductivity.[1] Thus, future solid-state batteries are expected to have faster charge and discharge as compared to the commercial lithium-ion batteries known today. Furthermore, hydridoborates are stable towards metallic anodes and have a tendency for increasing oxidative stability with increasing number of boron atoms in the anion. Thus, tetrahydridoborate has a relatively low oxidative stability but tends to be oxidised to *closo*-borates, *e.g.* $B_{12}H_{12}^{2-}$.[246] As an example, lithium tetrahydridoborate, $LiBH_4$, can be oxidised to form $Li_2B_{12}H_{12}$, which may dimerise to $B_{24}H_{23}^{3-}$ or trimerize to $B_{36}H_{34}^{4-}$ polyanions. Metal hydridoborates are known to have low material density, which contributes to increasing the energy densities of the electrochemical cell.[247] Metal hydridoborates are soft and compactable materials, with high deformability and good ability to form interfaces with good contact towards electrodes, *e.g.* upon mechanical cold pressing.[158] They are also known to have high chemical stability and are compatible with halides and oxides and can form double anion compounds such as $Ag_3(B_{12}H_{12})I$ and $LiCa_3(BH_4)(BO_3)_2$.[248,249] Metal hydridoborates have high stability towards halides and oxides and provide a variety of possible combinations with known electrolytes. This highlights hydridoborates as a very promising class of solid-state electrolytes with a range of prolific properties, which may be the foundation for future solid-state batteries.

Conflicts of interest

There are no conflicts to declare.

Data availability

Data for this review article are available *via* the references in the reference list in the manuscript. All of the information used in this review has been fully published. No primary research results have been included and no new data were generated or analysed as part of this review.

Acknowledgements

The authors acknowledge the important contribution of the International Energy Agency (IEA) Hydrogen Technology Collaboration Programme (TCP) Task 51: Hydrogen Materials for Energy. T. R. J. gratefully acknowledges support from the independent research fund Denmark for technology and production *via* Calcium Metal Battery – CaMBat (DFF – 0217-00327B) and affiliation with the Center for Integrated Materials Research (iMAT) at Aarhus University. Aarhus Universitets Forskningsfond (AUFF-F-2024-6-8) is acknowledged for support. C. E. B., M. P. and T. D. H. would like to thank the Australian Renewable Energy Agency (ARENA) for Transformative Research Accelerating Commercialisation (TRAC) Program grant 2023/TRAC005 (PRO-1081). M. D. gratefully acknowledges the support from the Leverhulme Trust International Professorship Program grant (LIP-2021-018) and the ISPF UK-Japan Advanced Materials Programme UKRI664. Y. F. acknowledges FNRS (CC J.0078.24) and SPW-Economie Emploi Recherche for Win4Excellence project "TiNTHyN" under contract No. 2310142. Marek Polanski would like to acknowledge the National Centre of Science, Poland (2021/43/B/ST5/01299).

References

1 J. B. Grinderslev, M. B. Amdisen, L. N. Skov, K. T. Møller, L. G. Kristensen, M. Polanski, M. Heere and T. R. Jensen, *J. Alloys Compd.*, 2022, **896**, 163014.
2 F. Cuevas, M. B. Amdisen, M. Baricco, C. E. Buckley, Y. W. Cho, P. de Jongh, L. M. de Kort, J. B. Grinderslev, V. Gulino, B. C. Hauback, M. Heere, T. Humphries, T. R. Jensen, S. Kim, K. Kisu, Y.-S. Lee, H.-W. Li, R. Mohtadi, K. T. Møller, P. Ngene, D. Noréus, S. Orimo, M. Paskevicius, M. Polanski, S. Sartori, L. N. Skov,

M. H. Sørby, B. C. Wood, V. A. Yartys, M. Zhu and M. Latroche, *Prog. Energy*, 2022, **4**, 032001.
3 L. Pasquini, K. Sakaki, E. Akiba, M. D. Allendorf, E. Alvares, J. R. Ares, D. Babai, M. Baricco, J. Bellosta von Colbe, M. Bereznitsky, C. E. Buckley, Y. W. Cho, F. Cuevas, P. de Rango, E. M. Dematteis, R. V. Denys, M. Dornheim, J. F. Fernández, A. Hariyadi, B. C. Hauback, T. W. Heo, M. Hirscher, T. D. Humphries, J. Huot, I. Jacob, T. R. Jensen, P. Jerabek, S. Y. Kang, N. Keilbart, H. Kim, M. Latroche, F. Leardini, H. Li, S. Ling, M. V. Lototskyy, R. Mullen, S. Orimo, M. Paskevicius, C. Pistidda, M. Polanski, J. Puszkiel, E. Rabkin, M. Sahlberg, S. Sartori, A. Santhosh, T. Sato, R. Z. Shneck, M. H. Sørby, Y. Shang, V. Stavila, J.-Y. Suh, S. Suwarno, L. Thi Thu, L. F. Wan, C. J. Webb, M. Witman, C. Wan, B. C. Wood and V. A. Yartys, *Prog. Energy*, 2022, **4**, 032007.
4 E. M. Dematteis, M. B. Amdisen, T. Autrey, J. Barale, M. E. Bowden, C. E. Buckley, Y. W. Cho, S. Deledda, M. Dornheim, P. de Jongh, J. B. Grinderslev, G. Gizer, V. Gulino, B. C. Hauback, M. Heere, T. W. Heo, T. D. Humphries, T. R. Jensen, S. Y. Kang, Y.-S. Lee, H.-W. Li, S. Li, K. T. Møller, P. Ngene, S. Orimo, M. Paskevicius, M. Polanski, S. Takagi, L. Wan, B. C. Wood, M. Hirscher and M. Baricco, *Prog. Energy*, 2022, **4**, 032009.
5 M. Adams, C. E. Buckley, M. Busch, R. Bunzel, M. Felderhoff, T. W. Heo, T. D. Humphries, T. R. Jensen, J. Klug, K. H. Klug, K. T. Møller, M. Paskevicius, S. Peil, K. Peinecke, D. A. Sheppard, A. D. Stuart, R. Urbanczyk, F. Wang, G. S. Walker, B. C. Wood, D. Weiss and D. M. Grant, *Prog. Energy*, 2022, **4**, 032008.
6 M. D. Allendorf, V. Stavila, J. L. Snider, M. Witman, M. E. Bowden, K. Brooks, B. L. Tran and T. Autrey, *Nat. Chem.*, 2022, **14**, 1214–1223.
7 M. Hirscher, V. A. Yartys, M. Baricco, J. Bellosta von Colbe, D. Blanchard, R. C. Bowman, D. P. Broom, C. E. Buckley, F. Chang, P. Chen, Y. W. Cho, J.-C. Crivello, F. Cuevas, W. I. F. David, P. E. de Jongh, R. V. Denys, M. Dornheim, M. Felderhoff, Y. Filinchuk, G. E. Froudakis, D. M. Grant, E. M. Gray, B. C. Hauback, T. He, T. D. Humphries, T. R. Jensen, S. Kim, Y. Kojima, M. Latroche, H.-W. Li, M. V. Lototskyy, J. W. Makepeace, K. T. Møller, L. Naheed, P. Ngene, D. Noréus, M. M. Nygård, S. Orimo, M. Paskevicius, L. Pasquini, D. B. Ravnsbæk, M. Veronica Sofianos, T. J. Udovic, T. Vegge, G. S. Walker, C. J. Webb, C. Weidenthaler and C. Zlotea, *J. Alloys Compd.*, 2020, **827**, 153548.
8 K. Yvon, in *Encyclopedia of Materials: Science and Technology*, ed. K. H. J. Buschow, R. W. Cahn, M. C. Flemings, B. Ilschner, E. J. Kramer, S. Mahajan and P. Veyssière, Elsevier, Oxford, 2004, pp. 1–9, DOI: 10.1016/B0-08-043152-6%2F01905-7.
9 T. D. Humphries, D. A. Sheppard and C. E. Buckley, *Coord. Chem. Rev.*, 2017, **342**, 19–33.
10 M. Paskevicius, L. H. Jepsen, P. Schouwink, R. Cerny, D. B. Ravnsbaek, Y. Filinchuk, M. Dornheim, F. Besenbacher and T. R. Jensen, *Chem. Soc. Rev.*, 2017, **46**, 1565–1634.
11 M. Bowden, D. J. Heldebrant, A. Karkamkar, T. Proffen, G. K. Schenter and T. Autrey, *Chem. Commun.*, 2010, **46**, 8564–8566.
12 A. Karkamkar, S. M. Kathmann, G. K. Schenter, D. J. Heldebrant, N. Hess, M. Gutowski and T. Autrey, *Chem. Mater.*, 2009, **21**, 4356–4358.
13 J. B. Grinderslev and T. R. Jensen, *Dalton Trans.*, 2022, **51**, 17762–17771.
14 S. Di Cataldo, C. Heil, W. von der Linden and L. Boeri, *Phys. Rev. B*, 2021, **104**, L020511.
15 A. Baran, M. Knioła, T. Rogala and M. Polanski, *Int. J. Hydrogen Energy*, 2022, **47**, 35003–35016.
16 D. J. Wolstenholme, J. L. Dobson and G. S. McGrady, *Dalton Trans.*, 2015, **44**, 9718–9731.
17 Y. Yan, W. Dononelli, M. Jorgensen, J. B. Grinderslev, Y.-S. Lee, Y. W. Cho, R. Černý, B. Hammer and T. R. Jensen, *Phys. Chem. Chem. Phys.*, 2020, **22**, 9204–9209.
18 L. H. Jepsen, Y. S. Lee, R. Černý, R. S. Sarusie, Y. W. Cho, F. Besenbacher and T. R. Jensen, *ChemSusChem*, 2015, **8**, 3472–3482.
19 R. C. Lochan and M. Head-Gordon, *Phys. Chem. Chem. Phys.*, 2006, **8**, 1357–1370.
20 D. P. Broom, C. J. Webb, K. E. Hurst, P. A. Parilla, T. Gennett, C. M. Brown, R. Zacharia, E. Tylianakis, E. Klontzas, G. E. Froudakis, T. A. Steriotis, P. N. Trikalitis, D. L. Anton, B. Hardy, D. Tamburello, C. Corgnale, B. A. van Hassel, D. Cossement, R. Chahine and M. Hirscher, *Appl. Phys. A*, 2016, **122**, 151–171.
21 D. P. Broom, C. J. Webb, G. S. Fanourgakis, G. E. Froudakis, P. N. Trikalitis and M. Hirscher, *Int. J. Hydrogen Energy*, 2019, **44**, 7768–7779.
22 J. A. Villajos, M. Bienert, N. Gugin, F. Emmerling and M. Maiwald, *Mater. Adv.*, 2023, **4**, 4226–4237.
23 D. Chakraborty, A. Yurdusen, G. Mouchaham, F. Nouar and C. Serre, *Adv. Funct. Mater.*, 2023, **34**, 2309089.
24 K. K. Gangu, S. Maddila and S. B. Jonnalagadda, *RSC Adv.*, 2022, **12**, 14282–14298.
25 T. Zhao, S. Nie, M. Luo, P. Xiao, M. Zou and Y. Chen, *J. Alloys Compd.*, 2024, **974**, 172897.
26 W. Luo, Z. Zhang, G. Zhu, X. Zhang, G. Huang, T. Zhou and X. Lu, *J. Environ. Chem. Eng.*, 2025, **13**, 118229.
27 C. Xu, J. Yang, M. Veenstra, A. Sudik, J. J. Purewal, Y. Ming, B. J. Hardy, J. Warner, S. Maurer, U. Müeller and D. J. Siegel, *Int. J. Hydrogen Energy*, 2013, **38**, 3268–3274.
28 L. Zhang, M. D. Allendorf, R. Balderas-Xicohténcatl, D. P. Broom, G. S. Fanourgakis, G. E. Froudakis, T. Gennett, K. E. Hurst, S. Ling, C. Milanese, P. A. Parilla, D. Pontiroli, M. Riccò, S. Shulda, V. Stavila, T. A. Steriotis, C. J. Webb, M. Witman and M. Hirscher, *Prog. Energy*, 2022, **4**, 042013.
29 A. R. Yuvaraj, A. Jayarama, D. Sharma, S. S. Nagarkar, S. P. Duttagupta and R. Pinto, *Int. J. Hydrogen Energy*, 2024, **59**, 1434–1458.
30 X. Zhang, P. Liu and Y. Zhang, *Inorg. Chim. Acta*, 2023, **557**, 121683.
31 R. Chahine and T. K. Bose, Proceedings: 11th World Hydrogen Energy Conference (WHEC), 1996, **2**, 1259–1263.
32 J. Huang, Y. Liang, H. Dong, H. Hu, P. Yu, L. Peng, M. Zheng, Y. Xiao and Y. Liu, *Int. J. Hydrogen Energy*, 2018, **43**, 18077–18082.
33 Y. Gogotsi, C. Portet, S. Osswald, J. M. Simmons, T. Yildirim, G. Laudisio and J. E. Fischer, *Int. J. Hydrogen Energy*, 2009, **34**, 6314–6319.
34 Y. Li, T. Ben, B. Zhang, Y. Fu and S. Qiu, *Sci. Rep.*, 2013, **3**, 2420.
35 A. Ahmed, S. Seth, J. Purewal, A. G. Wong-Foy, M. Veenstra, A. J. Matzger and D. J. Siegel, *Nat. Commun.*, 2019, **10**, 1568.
36 E. Poirier, *RSC Adv.*, 2014, **4**, 22848–22855.
37 L. Naheed, K. E. Lamb, E. M. Gray and C. J. Webb, *Adsorption*, 2021, **27**, 1251–1261.
38 M. P. Suh, H. J. Park, T. K. Prasad and D. W. Lim, *Chem. Rev.*, 2012, **112**, 782–835.
39 Y. E. Cheon and M. P. Suh, *Chem. Commun.*, 2009, 2296–2298.
40 Z. Wang, L. Sun, F. Xu, H. Zhou, X. Peng, D. Sun, J. Wang and Y. Du, *Int. J. Hydrogen Energy*, 2016, **41**, 8489–8497.
41 M. Jordá-Beneyto, D. Lozano-Castelló, F. Suárez-García, D. Cazorla-Amorós and A. Linares-Solano, *Microporous Mesoporous Mater.*, 2008, **112**, 235–242.
42 S. E. Bambalaza, H. W. Langmi, R. Mokaya, N. M. Musyoka, J. Ren and L. E. Khotseng, *J. Mater. Chem. A*, 2018, **6**, 23569–23577.
43 D. G. Madden, D. O'Nolan, N. Rampal, R. Babu, C. Camur, A. N. Al Shakhs, S. Y. Zhang, G. A. Rance, J. Perez, N. P. Maria Casati, C. Cuadrado-Collados, D. O'Sullivan, N. P. Rice, T. Gennett, P. Parilla, S. Shulda, K. E. Hurst, V. Stavila, M. D. Allendorf, J. Silvestre-Albero, A. C. Forse, N. R. Champness, K. W. Chapman and D. Fairen-Jimenez, *J. Am. Chem. Soc.*, 2022, **144**, 13729–13739.
44 A. J. A. Abubakar, R. L. S. Canevesi, D. A. L. Sanchez and C. A. Grande, *Chem. Eng. J.*, 2024, **489**, 151450.
45 M. D. Allendorf, Z. Hulvey, T. Gennett, A. Ahmed, T. Autrey, J. Camp, E. Seon Cho, H. Furukawa, M. Haranczyk, M. Head-Gordon, S. Jeong, A. Karkamkar, D.-J. Liu, J. R. Long, K. R. Meihaus, I. H. Nayyar, R. Nazarov, D. J. Siegel, V. Stavila, J. J. Urban, S. P. Veccham and B. C. Wood, *Energy Environ. Sci.*, 2018, **11**, 2784–2812.
46 Y. Filinchuk, B. Richter, T. R. Jensen, V. Dmitriev, D. Chernyshov and H. Hagemann, *Angew. Chem., Int. Ed.*, 2011, **50**, 11162–11166.
47 H. Oh, N. Tumanov, V. Ban, X. Li, B. Richter, M. R. Hudson, C. M. Brown, G. N. Iles, D. Wallacher, S. W. Jorgensen, L. Daemen, R. Balderas-Xicohténcatl, Y. Cheng, A. J. Ramirez-Cuesta, M. Heere, S. Posada-Pérez, G. Hautier, M. Hirscher, T. R. Jensen and Y. Filinchuk, *Nat. Chem.*, 2024, **16**, 809–816.
48 R. Hazen, H. Mao, L. Finger and R. Hemley, *Phys. Rev. B:Condens. Matter Mater. Phys.*, 1987, **36**, 3944.
49 I. Dovgaliuk, V. Dyadkin, M. V. Donckt, Y. Filinchuk and D. Chernyshov, *ACS Appl. Mater. Interfaces*, 2020, **12**, 7710–7716.
50 I. Dovgaliuk, I. Senkovska, X. Li, V. Dyadkin, Y. Filinchuk and D. Chernyshov, *Angew. Chem., Int. Ed.*, 2021, **60**, 5250–5256.

51 A. V. Skripov, M. Dimitrievska, O. A. Babanova, R. V. Skoryunov, A. V. Soloninin, F. Morelle, Y. Filinchuk, A. Faraone, H. Wu, W. Zhou and T. J. Udovic, *J. Phys. Chem. C*, 2019, **123**, 20789–20799.
52 M. Reberc, M. Mazaj, J. Stare, M. Počkaj, G. Mali, X. Li, Y. Filinchuk, R. Černý and A. Meden, *Inorg. Chem.*, 2022, **61**, 12708–12718.
53 L. A. M. Mahmoud, J. L. Rowlandson, D. J. Fermin, V. P. Ting and S. Nayak, *RSC Appl. Interfaces*, 2025, **2**, 25–55.
54 K. Mondal, S. J. Malode, N. P. Shetti, S. A. Alqarni, S. Pandiaraj and A. Alodhayb, *J. Energy Storage*, 2024, **76**, 109719.
55 D. E. Jaramillo, H. Z. H. Jiang, H. A. Evans, R. Chakraborty, H. Furukawa, C. M. Brown, M. Head-Gordon and J. R. Long, *J. Am. Chem. Soc.*, 2021, **143**, 6248–6256.
56 W. A. Braunecker, S. Shulda, M. B. Martinez, K. E. Hurst, J. T. Koubek, S. Zaccarine, R. E. Mow, S. Pylypenko, A. Sellinger, T. Gennett and J. C. Johnson, *ACS Mater. Lett.*, 2020, **2**, 227–232.
57 Y. Yabuuchi, H. Furukawa, K. M. Carsch, R. A. Klein, N. V. Tkachenko, A. J. Huang, Y. Cheng, K. M. Taddei, E. Novak, C. M. Brown, M. Head-Gordon and J. R. Long, *J. Am. Chem. Soc.*, 2024, **146**, 22759–22776.
58 D. Senthil Raja and D. H. Tsai, *Chem. Commun.*, 2024, **60**, 8497–8515.
59 Q. Fu, W. Niu, L. Yan, W. Xie, H. Jiang, S. Zhang, L. Yang, Y. Wang, Y. Xing and X. Zhao, *Mater. Lett.*, 2023, **343**, 134344.
60 H.-Y. Wu, C.-L. Wu, W. Liao, B. M. Matsagar, K.-Y. Chang, J.-H. Huang and K. C. W. Wu, *J. Mater. Chem. A*, 2023, **11**, 9427–9435.
61 L. Qiao, C. Lu, W. Fan, Z. Xue, X. Wang, Z. Kang and D. Sun, *Int. J. Hydrogen Energy*, 2024, **93**, 805–821.
62 S. Elyasi, S. Saha, N. Hameed, P. J. Mahon, S. Juodkazis and N. Salim, *Int. J. Hydrogen Energy*, 2024, **62**, 272–306.
63 J. Serafin, B. Dziejarski, C. Solis, P. Ramírez de la Piscina and N. Homs, *Fuel*, 2024, **363**, 130975.
64 E. Tsalaporta and J. M. D. MacElroy, *Heliyon*, 2020, **6**, e04883.
65 Y. Ming, J. Purewal, J. Yang, C. Xu, M. Veenstra, M. Gaab, U. Müller and D. J. Siegel, *Int. J. Hydrogen Energy*, 2016, **41**, 9374–9382.
66 T. C. Wang, J. L. White, B. Bie, H. Deng, J. Edgington, J. D. Sugar, V. Stavila and M. D. Allendorf, *ChemPhysChem*, 2019, **20**, 1305–1310.
67 J. Farrando-Pérez, M. Rodríguez-Castillo, M. Martínez-Escandell, M. Monge and J. Silvestre-Albero, *Int. J. Hydrogen Energy*, 2023, **48**, 36474–36484.
68 D. Menard, X. Py and N. Mazet, *Chem. Eng. Process. Process Intensif.*, 2005, **44**, 1029–1038.
69 D. Liu, J. J. Purewal, J. Yang, A. Sudik, S. Maurer, U. Mueller, J. Ni and D. J. Siegel, *Int. J. Hydrogen Energy*, 2012, **37**, 6109–6117.
70 S. E. Bambalaza, H. W. Langmi, N. M. Musyoka, J. Ren and L. E. Khotseng, *Mater. Today Proc.*, 2018, **5**, 10431–10439.
71 M. C. Tapia, B. G. Alamani and T.-H. Bae, *Sep. Purif. Technol.*, 2025, **363**, 132313.
72 H. Wang and D. C. Miller, *J. Electrochem. Eng. Conv. Stor.*, 2022, **19**, 011002.
73 S. Wang, M. Gao, Z. Yao, Y. Liu, M. Wu, Z. Li, Y. Liu, W. Sun and H. Pan, *Chem. Eng. J.*, 2022, **428**, 131056.
74 J.-Q. Hu, W. Jiang, N. Si, Z. Wang and H. Zhang, *Int. J. Hydrogen Energy*, 2024, **86**, 445–455.
75 Z. Yu, J. Deschamps, L. Hamon, P. Karikkethu Prabhakaran and P. Pré, *Int. J. Hydrogen Energy*, 2017, **42**, 8021–8031.
76 L. Luo, Y. Zhou, W. Yan, L. Luo, J. Deng, M. Fan and W. Zhao, *Int. J. Hydrogen Energy*, 2022, **47**, 39563–39571.
77 P. Ramirez-Vidal, G. Sdanghi, A. Celzard and V. Fierro, *Int. J. Hydrogen Energy*, 2022, **47**, 8892–8915.
78 T. K. Nielsen, A. Karkamkar, M. Bowden, F. Besenbacher, T. R. Jensen and T. Autrey, *Dalton Trans.*, 2013, **42**, 680–687.
79 V. Sit, R. Geanangel and W. Wendlandt, *Thermochim. Acta*, 1987, **113**, 379–382.
80 M. S. Andersson, J. B. Grinderslev, T. R. Jensen, V. García Sakai, U. Häussermann, T. J. Udovic and M. Karlsson, *Phys. Rev. Mater.*, 2020, **4**, 085002.
81 P. Schouwink, M. B. Ley, A. Tissot, H. Hagemann, T. R. Jensen, Ľ. Smrčok and R. Černý, *Nat. Commun.*, 2014, **5**, 5706.
82 P. Schouwink, F. Morelle, Y. Sadikin, Y. Filinchuk and R. Černý, *Energies*, 2015, **8**, 8286–8299.
83 J. B. Grinderslev, L. H. Jepsen, Y.-S. Lee, K. T. Møller, Y. W. Cho, R. Černý and T. R. Jensen, *Inorg. Chem.*, 2020, **59**, 12733–12747.
84 S. Filippov, J. B. Grinderslev, M. S. Andersson, J. Armstrong, M. Karlsson, T. R. Jensen, J. Klarbring, S. I. Simak and U. Häussermann, *J. Phys. Chem. C*, 2019, **123**, 28631–28639.
85 J. B. Grinderslev, Y.-S. Lee, M. Paskevicius, K. T. Møller, Y. Yan, Y. W. Cho and T. R. Jensen, *Inorg. Chem.*, 2020, **59**, 11449–11458.
86 D. R. Lide, *CRC Handbook of Chemistry and Physics*, CRC Press, Boca Raton, USA, New York, 88th edn, 2007.
87 M. Dornheim, N. Eigen, G. Barkhordarian, T. Klassen and R. Bormann, *Adv. Eng. Mater.*, 2006, **8**, 377–385.
88 M. B. Smith and G. E. Bass Jr, *J. Chem. Eng. Data*, 1963, **8**, 342–346.
89 F. Marques, M. Balcerzak, F. Winkelmann, G. Zepon and M. Felderhoff, *Energy Environ. Sci.*, 2021, **14**, 5191–5227.
90 T. R. Somo, M. V. Lototskyy, V. A. Yartys, M. W. Davids and S. N. Nyamsi, *J. Energy Storage*, 2023, **73**, 108969.
91 G. Zepon, B. H. Silva, C. Zlotea, W. J. Botta and Y. Champion, *Acta Mater.*, 2021, **215**, 117070.
92 M. Witman, G. Ek, S. Ling, J. Chames, S. Agarwal, J. Wong, M. D. Allendorf, M. Sahlberg and V. Stavila, *Chem. Mater.*, 2021, **33**, 4067–4076.
93 A. Agafonov, N. Pineda-Romero, M. Witman, V. Nassif, G. B. M. Vaughan, L. Lei, S. Ling, D. M. Grant, M. Dornheim, M. Allendorf, V. Stavila and C. Zlotea, *Acta Mater.*, 2024, **276**, 120086.
94 L. Kong, B. Cheng, D. Wan and Y. Xue, *Front. Mater.*, 2023, **10**, 1135864.
95 H. Ma and C. H. Shek, *J. Alloys Compd.*, 2020, **827**, 154159.
96 Y. Long, X. Liang, K. Su, H. Peng and X. Li, *J. Alloys Compd.*, 2019, **780**, 607–617.
97 A. Agafonov, N. Pineda-Romero, M. D. Witman, V. Enblom, M. Sahlberg, V. Nassif, L. Lei, D. M. Grant, M. Dornheim, S. Ling, V. Stavila and C. Zlotea, *ACS Appl. Mater. Interfaces*, 2025, **17**, 41991–42003.
98 Z. Wang, S. Chen, S. Yang, Q. Luo, Y. Jin, W. Xie, L. Zhang and Q. Li, *J. Mater. Sci. Technol.*, 2023, **151**, 41–65.
99 K. Chen, M. Y. Lau, X. Luo, J. Huang, L. Ouyang and X.-S. Yang, *J. Mater. Sci. Technol.*, 2026, **246**, 256–289.
100 M. M. Nygård, Ø. S. Fjellvåg, M. H. Sørby, K. Sakaki, K. Ikeda, J. Armstrong, P. Vajeeston, W. A. Sławiński, H. Kim, A. Machida, Y. Nakamura and B. C. Hauback, *Acta Mater.*, 2021, **205**, 116496.
101 B. Cheng, L. Kong, H. Cai, Y. Li, Y. Zhao, D. Wan and Y. Xue, *Int. J. Hydrogen Energy*, 2024, **60**, 282–292.
102 M. Dornheim, L. Baetcke, E. Akiba, J.-R. Ares, T. Autrey, J. Barale, M. Baricco, K. Brooks, N. Chalkiadakis, V. Charbonnier, S. Christensen, J. Bellosta von Colbe, M. Costamagna, E. Dematteis, J.-F. Fernández, T. Gennett, D. Grant, T. W. Heo, M. Hirscher, K. Hurst, M. Lototskyy, O. Metz, P. Rizzi, K. Sakaki, S. Sartori, E. Stamatakis, A. Stuart, A. Stubos, G. Walker, C. J. Webb, B. Wood, V. Yartys and E. Zoulias, *Prog. Energy*, 2022, **4**, 042005.
103 V. A. Yartys, M. V. Lototskyy, V. Linkov, S. Pasupathi, M. W. Davids, I. Tolj, G. Radica, R. V. Denys, J. Eriksen, K. Taube, J. Bellosta von Colbe, G. Capurso, M. Dornheim, F. Smith, D. Mathebula, D. Swanepoel and S. Suwarno, *Int. J. Hydrogen Energy*, 2021, **46**, 35896–35909.
104 J. C. Crivello, R. V. Denys, M. Dornheim, M. Felderhoff, D. M. Grant, J. Huot, T. R. Jensen, P. de Jongh, M. Latroche, G. S. Walker, C. J. Webb and V. A. Yartys, *Appl. Phys. A*, 2016, **122**, 85–101.
105 V. A. Yartys, M. V. Lototskyy, E. Akiba, R. Albert, V. E. Antonov, J. R. Ares, M. Baricco, N. Bourgeois, C. E. Buckley, J. M. Bellosta von Colbe, J. C. Crivello, F. Cuevas, R. V. Denys, M. Dornheim, M. Felderhoff, D. M. Grant, B. C. Hauback, T. D. Humphries, I. Jacob, T. R. Jensen, P. E. de Jongh, J. M. Joubert, M. A. Kuzovnikov, M. Latroche, M. Paskevicius, L. Pasquini, L. Popilevsky, V. M. Skripnyuk, E. Rabkin, M. V. Sofianos, A. Stuart, G. Walker, H. Wang, C. J. Webb and M. Zhu, *Int. J. Hydrogen Energy*, 2019, **44**, 7809–7859.
106 A.-L. Chaudhary, S. Dietzel, H.-W. Li, E. Akiba, N. Bergemann, C. Pistidda, T. Klassen and M. Dornheim, *Int. J. Hydrogen Energy*, 2017, **42**, 11422–11428.
107 M. Dornheim, S. Doppiu, G. Barkhordarian, U. Boesenberg, T. Klassen, O. Gutfleisch and R. Bormann, *Scripta Mater.*, 2007, **56**, 841–846.
108 C. J. Webb, *J. Phys. Chem. Solids*, 2015, **84**, 96–106.
109 B. Bogdanović and M. Schwickardi, *J. Alloys Compd.*, 1997, **253–254**, 1–9.

110 L. Mosegaard, B. Møller, J.-E. Jørgensen, U. Bösenberg, M. Dornheim, J. C. Hanson, Y. Cerenius, G. Walker, H. J. Jakobsen, F. Besenbacher and T. R. Jensen, *J. Alloys Compd.*, 2007, **446–447**, 301–305.
111 G. Li, M. Matsuo, S. Takagi, A.-L. Chaudhary, T. Sato, M. Dornheim and S. Orimo, *Inorganics*, 2017, **5**, 81.
112 G. Barkhordarian, T. Klassen, M. Dornheim and R. Bormann, *J. Alloys Compd.*, 2007, **440**, L18–L21.
113 N. Kuganathan, M. Dornheim, D. M. Grant and S. Ling, *Mater. Chem. Phys.*, 2024, **324**, 129677.
114 J. J. Vajo, F. Mertens, C. C. Ahn, R. C. Bowman and B. Fultz, *J. Phys. Chem. B*, 2004, **108**, 13977–13983.
115 T. T. Le, C. Pistidda, V. H. Nguyen, P. Singh, P. Raizada, T. Klassen and M. Dornheim, *Int. J. Hydrogen Energy*, 2021, **46**, 23723–23736.
116 R. Utke, S. Thiangviriya, P. Javadian, T. R. Jensen, C. Milanese, T. Klassen and M. Dornheim, *Mater. Chem. Phys.*, 2016, **169**, 136–141.
117 N. Bergemann, C. Pistidda, M. Uptmoor, C. Milanese, A. Santoru, T. Emmler, J. Puszkiel, M. Dornheim and T. Klassen, *J. Energy Chem.*, 2019, **34**, 240–254.
118 J. J. Vajo, W. Li and P. Liu, *Chem. Commun.*, 2010, **46**, 6687–6689.
119 P. Dansirima, J. B. Grinderslev, L. G. Kristensen, R. Utke and T. R. Jensen, *Int. J. Hydrogen Energy*, 2025, **98**, 908–914.
120 F. Karimi, S. Börries, P. K. Pranzas, O. Metz, A. Hoell, G. Gizer, J. A. Puszkiel, M. V. C. Riglos, C. Pistidda, M. Dornheim, T. Klassen and A. Schreyer, *Adv. Eng. Mater.*, 2021, **23**, 2100294.
121 F. Karimi, M. V. C. Riglos, A. Santoru, A. Hoell, V. S. Raghuwanshi, C. Milanese, N. Bergemann, C. Pistidda, P. Nolis, M. D. Baro, G. Gizer, T.-T. Le, P. K. Pranzas, M. Dornheim, T. Klassen, A. Schreyer and J. Puszkiel, *J. Phys. Chem. C*, 2018, **122**, 11671–11681.
122 Z. Xiong, J. Hu, G. Wu, P. Chen, W. Luo, K. Gross and J. Wang, *J. Alloys Compd.*, 2005, **398**, 235–239.
123 G. Gizer, J. Puszkiel, H. Cao, C. Pistidda, T. T. Le, M. Dornheim and T. Klassen, *Int. J. Hydrogen Energy*, 2019, **44**, 11920–11929.
124 H. Wang, G. Wu, H. Cao, C. Pistidda, A. L. Chaudhary, S. Garroni, M. Dornheim and P. Chen, *Adv. Energy Mater.*, 2017, **7**, 1602456.
125 S. Orimo, Y. Nakamori and A. Zuttel, *Mater. Sci. Eng., B*, 2004, **108**, 51–53.
126 M. Paskevicius, M. B. Ley, D. A. Sheppard, T. R. Jensen and C. E. Buckley, *Phys. Chem. Chem. Phys.*, 2013, **15**, 19774–19789.
127 P. Martelli, R. Caputo, A. Remhof, P. Mauron, A. Borgschulte and A. Züttel, *J. Phys. Chem. C*, 2010, **114**, 7173–7177.
128 D. S. Stasinevich and G. A. Egorenko, *Russ. J. Inorg. Chem.*, 1968, **13**, 341–343.
129 T. D. Humphries, G. N. Kalantzopoulos, I. Llamas-Jansa, J. E. Olsen and B. C. Hauback, *J. Phys. Chem. C*, 2013, **117**, 6060–6065.
130 H. I. Schlesinger, H. C. Brown, H. R. Hoekstra and L. R. Rapp, *J. Am. Chem. Soc.*, 1953, **75**, 199–204.
131 H. N. Abdelhamid, *Int. J. Hydrogen Energy*, 2021, **46**, 726–765.
132 L. Ouyang, J. Jiang, K. Chen, M. Zhu and Z. Liu, *Nano-Micro Lett.*, 2021, **13**, 134.
133 U. B. Demirci, *Int. J. Hydrogen Energy*, 2023, **48**, 29682–29698.
134 A. Ibrahim, M. Paskevicius and C. E. Buckley, *Sustain. Energy Fuels*, 2023, **7**, 1196–1203.
135 A. Ibrahim, M. Paskevicius, A. Patel, A. M. D'Angelo, T. D. Humphries and C. E. Buckley, *ACS Appl. Energy Mater.*, 2024, **7**, 11206–11217.
136 H. X. Nunes, D. L. Silva, C. M. Rangel and A. M. F. R. Pinto, *Energies*, 2021, **14**, 3567.
137 Y. Liu, M. Paskevicius, T. D. Humphries and C. E. Buckley, *Int. J. Hydrogen Energy*, 2022, **47**, 25347–25356.
138 Y. Kojima and T. Haga, *Int. J. Hydrogen Energy*, 2003, **28**, 989–993.
139 T. Ou, A. Giuliano, M. Panizza, A. Barbucci and G. Cerisola, *Int. J. Hydrogen Energy*, 2013, **38**, 15269–15274.
140 A. Patel, P. Ó. Conghaile, T. D. Humphries, M. Paskevicius and C. E. Buckley, *Next Energy*, 2025, **9**, 100364.
141 T. P. T. Nguyen, T. D. Humphries, H. Hagemann, C. E. Buckley, T. R. Jensen and M. Paskevicius, *Dalton Trans.*, 2025, **54**, 1199–1211.
142 M. Wang, W. Guo, S. Wang, Y. Guo, J. Yang and T. Deng, *J. Chem. Eng. Data*, 2020, **65**, 5184–5191.
143 M. Matsuo, Y. Nakamori, S. Orimo, H. Maekawa and H. Takamura, *Appl. Phys. Lett.*, 2007, **91**, 224103.
144 H. Maekawa, M. Matsuo, H. Takamura, M. Ando, Y. Noda, T. Karahashi and S. Orimo, *J. Am. Chem. Soc.*, 2009, **131**, 894–895.
145 Y. Yan, J. B. Grinderslev, M. Jorgensen, L. N. Skov, J. Skibsted and T. R. Jensen, *ACS Appl. Energy Mater.*, 2020, **3**, 9264–9270.
146 Y. Yan, J. B. Grinderslev, T. Burankova, S. Wei, J. P. Embs, J. Skibsted and T. R. Jensen, *J. Phys. Chem. Lett.*, 2022, **13**, 2211–2216.
147 L. N. Skov, J. B. Grinderslev and T. R. Jensen, *Batteries Supercaps*, 2023, **6**, e202300185.
148 M. B. Amdisen, J. B. Grinderslev, L. N. Skov and T. R. Jensen, *Chem. Mater.*, 2023, **35**, 1440–1448.
149 L. N. Skov, J. B. Grinderslev, A. Rosenkranz, Y. S. Lee and T. R. Jensen, *Batteries Supercaps*, 2022, **5**, e202200163.
150 L. G. Kristensen, M. B. Amdisen, L. N. Skov and T. R. Jensen, *Phys. Chem. Chem. Phys.*, 2022, **24**, 18185–18197.
151 Y. Yan, J. B. Grinderslev, Y.-S. Lee, M. Jørgensen, Y. W. Cho, R. Černý and T. R. Jensen, *Chem. Commun.*, 2020, **56**, 3971–3974.
152 R. Zhang, W. Zhao, Z. Liu, S. Wei, Y. Yan and Y. Chen, *Chem. Commun.*, 2021, **57**, 2380–2383.
153 W. Zhao, R. Zhang, H. Li, Y. Zhang, Y. Wang, C. Wu, Y. Yan and Y. Chen, *ACS Appl. Mater. Interfaces*, 2021, **13**, 31635–31641.
154 J. B. Grinderslev, L. N. Skov, J. G. Andreasen, S. Ghorwal, J. Skibsted and T. R. Jensen, *Angew. Chem., Int. Ed.*, 2022, **134**, e202203484.
155 M. B. Amdisen and T. R. Jensen, *Chem. Mater.*, 2025, **37**, 1183–1194.
156 L. N. Skov, J. B. Grinderslev, T. S. S. Kjaer, L. R. Kristensen and T. R. Jensen, *Angew. Chem., Int. Ed.*, 2025, **64**, e202500613.
157 J. B. Grinderslev, L. N. Skov, L. R. Kristensen and T. R. Jensen, *Angew. Chem., Int. Ed.*, 2025, **64**, e202510493.
158 R. Černý, F. Murgia and M. Brighi, *J. Alloys Compd.*, 2022, **895**, 162659.
159 Z. Zhang and L. F. Nazar, *Nat. Rev. Mater.*, 2022, **7**, 389–405.
160 M. Paskevicius, M. P. Pitt, D. H. Brown, D. A. Sheppard, S. Chumphongphan and C. E. Buckley, *Phys. Chem. Chem. Phys.*, 2013, **15**, 15825–15828.
161 N. Verdal, J.-H. Her, V. Stavila, A. V. Soloninin, O. A. Babanova, A. V. Skripov, T. J. Udovic and J. J. Rush, *J. Solid State Chem.*, 2014, **212**, 81–91.
162 I. M. Riddlestone, A. Kraft, J. Schaefer and I. Krossing, *Angew. Chem., Int. Ed.*, 2018, **57**, 13982–14024.
163 T. P. T. Nguyen, W. Gao, T. D. Humphries, Y. Zhong, C. E. Buckley and M. Paskevicius, *J. Mater. Chem. A*, 2025, **13**, 28440–28450.
164 L. Duchêne, D. H. Kim, Y. B. Song, S. Jun, R. Moury, A. Remhof, H. Hagemann, Y. S. Jung and C. Battaglia, *Energy Storage Mater.*, 2020, **26**, 543–549.
165 G. Deysher, J. A. S. Oh, Y.-T. Chen, B. Sayahpour, S.-Y. Ham, D. Cheng, P. Ridley, A. Cronk, S. W.-H. Lin, K. Qian, L. H. B. Nguyen, J. Jang and Y. S. Meng, *Nat. Energy*, 2024, **9**, 1161–1172.
166 D. H. P. Souza, K. T. Møller, S. A. Moggach, T. D. Humphries, A. M. D'Angelo, C. E. Buckley and M. Paskevicius, *J. Mater. Chem. A*, 2021, **9**, 15027–15037.
167 D. H. P. Souza, T. D. Humphries, Y. Liu, A. Gradišek, A. M. D'Angelo, C. E. Buckley and M. Paskevicius, *Sustain. Energy Fuels*, 2022, **6**, 4614–4625.
168 D. H. P. Souza, A. M. D'Angelo, T. D. Humphries, C. E. Buckley and M. Paskevicius, *Dalton Trans.*, 2022, **51**, 13848–13857.
169 T. A. Hales, K. T. Møller, T. D. Humphries, A. M. D'Angelo, C. E. Buckley and M. Paskevicius, *J. Phys. Chem. C*, 2023, **127**, 949–957.
170 T. A. Hales, K. T. Møller, T. D. Humphries, A. M. D'Angelo, C. E. Buckley and M. Paskevicius, *Phys. Chem. Chem. Phys.*, 2023, **25**, 31249–31256.
171 S. R. H. Jensen, M. Jørgensen, T. P. T. Nguyen, G. Nolan, C. E. Buckley, T. R. Jensen and M. Paskevicius, *Dalton Trans.*, 2024, **53**, 7619–7627.
172 B. R. S. Hansen, M. Paskevicius, M. Jørgensen and T. R. Jensen, *Chem. Mater.*, 2017, **29**, 3423–3430.
173 M. Jørgensen, S. R. Jensen, T. D. Humphries, M. R. Rowles, M. V. Sofianos, C. E. Buckley, T. R. Jensen and M. Paskevicius, *J. Phys. Chem. C*, 2020, **124**, 11340–11349.
174 A. Berger, A. Ibrahim, T. A. Hales, A. M. D'Angelo, C. E. Buckley and M. Paskevicius, *Dalton Trans.*, 2024, **53**, 3638–3653.
175 M. Green, H. Simonyan, K. Kaydanik and J. A. Teprovich, *Appl. Sci.*, 2022, **12**, 2273.
176 H. Simonyan, L. Zhong, M. M. Green, K. Movsesyan, A. Fraire, P. A. Ward, K. C. Lau and J. A. Teprovich, Jr., *ACS Appl Mater Interfaces*, 2024, **16**, 70028–70037.

177 R. Mohtadi, M. Matsui, T. S. Arthur and S.-J. Hwang, *Angew. Chem., Int. Ed.*, 2012, **51**, 9780–9783.
178 I. Weber, J. Ingenmey, J. Schnaidt, B. Kirchner and R. J. Behm, *ChemElectroChem*, 2021, **8**, 390–402.
179 F. Tuerxun, K. Yamamoto, M. Hattori, T. Mandai, K. Nakanishi, A. Choudhary, Y. Tateyama, K. Sodeyama, A. Nakao, T. Uchiyama, M. Matsui, K. Tsuruta, Y. Tamenori, K. Kanamura and Y. Uchimoto, *ACS Appl. Mater. Interfaces*, 2020, **12**, 25775–25785.
180 S. Su, Y. NuLi, N. Wang, D. Yusipu, J. Yang and J. Wang, *J. Electrochem. Soc.*, 2016, **163**, D682.
181 D. Zhang, Y. Sun, X. Liu, Y. Zhang, R. Wang, Y. Zhao, M. Pan, Y. Wang, S. Chen, M. Zhou, Y. Chen, J. Yang, J. Wang and Y. NuLi, *ACS Energy Lett.*, 2024, **9**, 2685–2695.
182 N. T. Hahn, J. Self, K. S. Han, V. Murugesan, K. T. Mueller, K. A. Persson and K. R. Zavadil, *J. Phys. Chem. B*, 2021, **125**, 3644–3652.
183 T. Watkins, A. Kumar and D. A. Buttry, *J. Am. Chem. Soc.*, 2016, **138**, 641–650.
184 O. Tutusaus, R. Mohtadi, T. S. Arthur, F. Mizuno, E. G. Nelson and Y. V. Sevryugina, *Angew. Chem., Int. Ed.*, 2015, **54**, 7900–7904.
185 O. Tutusaus, R. Mohtadi, N. Singh, T. S. Arthur and F. Mizuno, *ACS Energy Lett.*, 2017, **2**, 224–229.
186 R. Jay, A. W. Tomich, J. Zhang, Y. Zhao, A. De Gorostiza, V. Lavallo and J. Guo, *ACS Appl. Mater. Interfaces*, 2019, **11**, 11414–11420.
187 H. Dong, O. Tutusaus, Y. Liang, Y. Zhang, Z. Lebens-Higgins, W. Yang, R. Mohtadi and Y. Yao, *Nat. Energy*, 2020, **5**, 1043–1050.
188 D. Wang, X. Gao, Y. Chen, L. Jin, C. Kuss and P. G. Bruce, *Nat. Mater.*, 2018, **17**, 16–20.
189 S. A. McClary, D. M. Long, A. Sanz-Matias, P. G. Kotula, D. Prendergast, K. L. Jungjohann and K. R. Zavadil, *ACS Energy Lett.*, 2022, **7**, 2792–2800.
190 A. M. Melemed, D. A. Skiba, K. J. Steinberg, K.-H. Kim and B. M. Gallant, *J. Phys. Chem. C*, 2023, **127**, 19886–19899.
191 Z. Yang, N. J. Leon, C. Liao, B. J. Ingram and L. Trahey, *ACS Appl. Mater. Interfaces*, 2023, **15**, 25018–25028.
192 K. Kisu, S. Kim, T. Shinohara, K. Zhao, A. Züttel and S. Orimo, *Sci. Rep.*, 2021, **11**, 7563.
193 H. N. M. Sarangika, H. T. G. Shashintha, M. A. K. L. Dissanayake and G. K. R. Senadeera, *J. Solid State Electrochem.*, 2024, **28**, 2163–2173.
194 Y. Shao, N. N. Rajput, J. Hu, M. Hu, T. Liu, Z. Wei, M. Gu, X. Deng, S. Xu, K. S. Han, J. Wang, Z. Nie, G. Li, K. R. Zavadil, J. Xiao, C. Wang, W. A. Henderson, J.-G. Zhang, Y. Wang, K. T. Mueller, K. Persson and J. Liu, *Nano Energy*, 2015, **12**, 750–759.
195 X. Zhang, T. Zhang, Y. Shao, H. Cao, Z. Liu, S. Wang and X. Zhang, *ACS Sustain. Chem. Eng.*, 2021, **9**, 5396–5404.
196 P. Wang, J. Trück, J. Häcker, A. Schlosser, K. Küster, U. Starke, L. Reinders and M. R. Buchmeiser, *Energy Storage Mater.*, 2022, **49**, 509–517.
197 T. Shinohara, K. Kisu, A. Dorai, K. Zushida, H. Yabu, S. Takagi and S. Orimo, *Adv. Sci.*, 2024, **11**, 2308318.
198 M. Green, K. Kaydanik, M. Orozco, L. Hanna, M. A. T. Marple, K. A. S. Fessler, W. B. Jones, V. Stavila, P. A. Ward and J. A. Teprovich Jr., *Adv. Sci.*, 2022, **9**, 2106032.
199 K. Bao, Y. Pang, J. Yang, D. Sun, F. Fang and S. Zheng, *Sci. China Mater.*, 2022, **65**, 95–104.
200 A. Du, H. Zhang, Z. Zhang, J. Zhao, Z. Cui, Y. Zhao, S. Dong, L. Wang, X. Zhou and G. Cui, *Adv. Mater.*, 2019, **31**, 1805930.
201 J. Guschlbauer, L. Niedzicki, L. Jacob, E. Rzeszotarska, D. Pociecha and P. Kaszyński, *J. Mol. Liq.*, 2023, **377**, 121525.
202 L. Jacob, L. Niedzicki, R. Jakubowski, D. Pociecha and P. Kaszyński, *Dalton Trans.*, 2024, **53**, 10293–10302.
203 E. Wigner and H. B. Huntington, *J. Chem. Phys.*, 1935, **3**, 764–770.
204 N. W. Ashcroft, *Phys. Rev. Lett.*, 1968, **21**, 1748–1749.
205 N. W. Ashcroft, *Phys. Rev. Lett.*, 2004, **92**, 187002.
206 F. Peng, Y. Sun, C. J. Pickard, R. J. Needs, Q. Wu and Y. Ma, *Phys. Rev. Lett.*, 2017, **119**, 107001.
207 A. P. Drozdov, P. P. Kong, V. S. Minkov, S. P. Besedin, M. A. Kuzovnikov, S. Mozaffari, L. Balicas, F. F. Balakirev, D. E. Graf, V. B. Prakapenka, E. Greenberg, D. A. Knyazev, M. Tkacz and M. I. Eremets, *Nature*, 2019, **569**, 528–531.
208 P. Kong, V. S. Minkov, M. A. Kuzovnikov, A. P. Drozdov, S. P. Besedin, S. Mozaffari, L. Balicas, F. F. Balakirev, V. B. Prakapenka, S. Chariton, D. A. Knyazev, E. Greenberg and M. I. Eremets, *Nat. Commun.*, 2021, **12**, 5075.
209 W. Chen, D. V. Semenok, X. Huang, H. Shu, X. Li, D. Duan, T. Cui and A. R. Oganov, *Phys. Rev. Lett.*, 2021, **127**, 117001.
210 D. V. Semenok, A. G. Kvashnin, A. G. Ivanova, V. Svitlyk, V. Y. Fominski, A. V. Sadakov, O. A. Sobolevskiy, V. M. Pudalov, I. A. Troyan and A. R. Oganov, *Mater. Today*, 2020, **33**, 36–44.
211 Z. Li, X. He, C. Zhang, X. Wang, S. Zhang, Y. Jia, S. Feng, K. Lu, J. Zhao, J. Zhang, B. Min, Y. Long, R. Yu, L. Wang, M. Ye, Z. Zhang, V. Prakapenka, S. Chariton, P. A. Ginsberg, J. Bass, S. Yuan, H. Liu and C. Jin, *Nat. Commun.*, 2022, **13**, 2863.
212 S. Mozaffari, D. Sun, V. S. Minkov, A. P. Drozdov, D. Knyazev, J. B. Betts, M. Einaga, K. Shimizu, M. I. Eremets, L. Balicas and F. F. Balakirev, *Nat. Commun.*, 2019, **10**, 2522.
213 F. Hong, P. F. Shan, L. X. Yang, B. B. Yue, P. T. Yang, Z. Y. Liu, J. P. Sun, J. H. Dai, H. Yu, Y. Y. Yin, X. H. Yu, J. G. Cheng and Z. X. Zhao, *Mater. Today Phys.*, 2022, **22**, 100596.
214 J. Bi, Y. Nakamoto, P. Zhang, K. Shimizu, B. Zou, H. Liu, M. Zhou, G. Liu, H. Wang and Y. Ma, *Nat. Commun.*, 2022, **13**, 5952.
215 L.-C. Chen, T. Luo, Z.-Y. Cao, P. Dalladay-Simpson, G. Huang, D. Peng, L.-L. Zhang, F. A. Gorelli, G.-H. Zhong, H.-Q. Lin and X.-J. Chen, *Nat. Commun.*, 2024, **15**, 1809.
216 D. V. Semenok, I. A. Troyan, A. G. Ivanova, A. G. Kvashnin, I. A. Kruglov, M. Hanfland, A. V. Sadakov, O. A. Sobolevskiy, K. S. Pervakov, I. S. Lyubutin, K. V. Glazyrin, N. Giordano, D. N. Karimov, A. L. Vasiliev, R. Akashi, V. M. Pudalov and A. R. Oganov, *Mater. Today*, 2021, **48**, 18–28.
217 S. Chen, Y. Wang, F. Bai, X. Wu, X. Wu, A. Pakhomova, J. Guo, X. Huang and T. Cui, *J. Am. Chem. Soc*, 2024, **146**, 14105–14113.
218 J. Bardeen, L. N. Cooper and J. R. Schrieffer, *Phys. Rev.*, 1957, **106**, 162–164.
219 J. E. Hirsch and F. Marsiglio, *Matter Radiat. Extremes*, 2022, **7**, 058401.
220 J. E. Hirsch, *Nat. Sci. Rev.*, 2023, **11**, nwad174.
221 P. Bhattacharyya, W. Chen, X. Huang, S. Chatterjee, B. Huang, B. Kobrin, Y. Lyu, T. J. Smart, M. Block, E. Wang, Z. Wang, W. Wu, S. Hsieh, H. Ma, S. Mandyam, B. Chen, E. Davis, Z. M. Geballe, C. Zu, V. Struzhkin, R. Jeanloz, J. E. Moore, T. Cui, G. Galli, B. I. Halperin, C. R. Laumann and N. Y. Yao, *Nature*, 2024, **627**, 73–79.
222 M. Du, H. Huang, Z. Zhang, M. Wang, H. Song, D. Duan and T. Cui, *Adv. Sci.*, 2024, **11**, 2408370.
223 K. Dolui, L. J. Conway, C. Heil, T. A. Strobel, R. P. Prasankumar and C. J. Pickard, *Phys. Rev. Lett.*, 2024, **132**, 166001.
224 S. Di Cataldo and L. Boeri, *Phys. Rev. B*, 2023, **107**, L060501.
225 N. Porcellino, C. Pakhanyan, T. Elmslie, M. Shivanna, S. Duwal, C. D. Spataru, R. Lindvall, M. Somayazulu, P. A. Ward, S. I. Kawaguchi, V. Stavila, P. A. Sharma and J. A. Teprovich, *ACS Appl. Energy Mater.*, 2024, **7**, 9608–9615.
226 M. Shivanna, T. A. Elmslie, C. D. Spataru, S. Duwal, N. Porcellino, S. Mouzaya, C. P. Pakhanyan, F. El Gabaly, S. Kawaguchi-Imada, J. Guo, Z. Zhuo, M.-J. Kim, B. T. Sturtevant, J. A. Teprovich, M. D. Allendorf, P. A. Sharma and V. Stavila, *ACS Appl. Energy Mater.*, 2024, **8**, 7–15.
227 H. Xu, O. Schneble, R. Jaramillo, M. Polanski and J. Li, *Phys. Rev. Lett.*, 2025, submitted.
228 J. Huot, F. Cuevas, S. Deledda, K. Edalati, Y. Filinchuk, T. Grosdidier, B. C. Hauback, M. Heere, T. R. Jensen, M. Latroche and S. Sartori, *Materials*, 2019, **12**, 2778.
229 R. A. Varin, R. Parviz, M. Polanski and Z. S. Wronski, *Int. J. Hydrogen Energy*, 2014, **39**, 10585–10599.
230 A. D. Katsenis, A. Puskaric, V. Strukil, C. Mottillo, P. A. Julien, K. Uzarevic, M. H. Pham, T. O. Do, S. A. Kimber, P. Lazic, O. Magdysyuk, R. E. Dinnebier, I. Halasz and T. Friscic, *Nat. Commun.*, 2015, **6**, 6662.
231 H. Li, J. Huang, K. Yang, Z. Lu, S. Yan, H. Su, C. Liu, X. Wang and B. Ren, *J. Phys. Chem. Lett.*, 2022, **13**, 479–485.
232 J. Batteas, K. G. Blank, E. Colacino, F. Emmerling, T. Friščić, J. Mack, J. Moore, M. E. Rivas and W. Tysoe, *RSC Mechanochem.*, 2025, **2**, 10–19.
233 V. Martinez, T. Stolar, B. Karadeniz, I. Brekalo and K. Užarević, *Nat. Rev. Chem.*, 2023, **7**, 51–65.
234 C. Pistidda, A. Santhosh, P. Jerabek, Y. Shang, A. Girella, C. Milanese, M. Dore, S. Garroni, S. Bordignon, M. R. Chierotti, T. Klassen and M. Dornheim, *J. Phys. Energy*, 2021, **3**, 044001.

235 A. K. Patel, D. Siemiaszko, J. Dworecka-Wójcik and M. Polański, *Int. J. Hydrogen Energy*, 2022, **47**, 5361–5371.
236 I. Wyrębska, K. Tomczyk, D. Siemiaszko, D. Zasada, J. Dworecka-Wójcik, M. Pęska, R. Chulist, S. Koter and M. Polański, *Chem. Eng. J.*, 2024, **485**, 149673.
237 T. Friscic, C. Mottillo and H. M. Titi, *Angew. Chem., Int. Ed.*, 2020, **59**, 1018–1029.
238 T. N. Dymova, Z. K. Sterlyadkina and V. G. Safronov, *Russ. J. Inorg. Chem.*, 1961, **6**, 389–395.
239 E. Wiberg, H. Goeltzer and R. Bauer, *Z. Naturforsch., B*, 1951, 394–395.
240 J. Huot, M.-L. Tremblay and R. Schulz, *J. Alloys Compd.*, 2003, **356**, 603–607.
241 A. Baran, T. R. Jensen and M. Polański, *Adv. Eng. Mater.*, 2024, **27**, 2400435.
242 A. Baran, T. R. Jensen and M. Polański, *J. Energy Storage*, 2024, **103**, 114271.
243 A. Baran, T. R. Jensen and M. Polański, *J. Energy Storage*, 2024, **103**, 114272.
244 L. Yu, R. Qu, S. Jiang, C. Hu, Y. Wang, L. Xu, S. Li and X. Du, *Renew. Sustain. Energy Rev.*, 2026, **225**, 116151.
245 H. Gudla, A. Hockmann, D. Brandell and J. Mindemark, *ACS Appl. Polym. Mater.*, 2025, **7**, 4716–4724.
246 R. Asakura, Z. Łodziana, R. Grissa, D. Rentsch, C. Battaglia and A. Remhof, *ACS Appl. Energy Mater.*, 2025, **8**, 9637–9645.
247 M. Brighi, F. Murgia and R. Černý, *Cell Rep. Phys. Sci.*, 2020, **1**, 100217.
248 M. Paskevicius, B. R. S. Hansen, M. Jorgensen, B. Richter and T. R. Jensen, *Nat Commun*, 2017, **8**, 15136.
249 Y.-S. Lee, Y. Filinchuk, H.-S. Lee, J.-Y. Suh, J. W. Kim, J.-S. Yu and Y. W. Cho, *J. Phys. Chem. C*, 2011, **115**, 10298–10304.